COMPOSITIONAL EFFECT ON LOW TEMPERATURE TRANSIENT LIQUID PHASE SINTERING OF TIN INDIUM SOLDER PASTE

by

John Obamedo

A Thesis

Submitted to the Faculty of Purdue University

In Partial Fulfillment of the Requirements for the degree of

Master of Science in Materials Engineering

School of Materials Engineering

West Lafayette, Indiana

December 2021

THE PURDUE UNIVERSITY GRADUATE SCHOOL
STATEMENT OF COMMITTEE APPROVAL

John E. Blendell
School of Materials Engineering

Carol A. Handwerker
School of Materials Engineering

Eric P. Kvam
School of Materials Engineering

Approved by:
Dr. David F. Bahr

TABLE OF CONTENTS

LIST OF TABLES

LIST OF FIGURES

ABSTRACT

Transient liquid phase sintering (TLPS) technologies are potential low-temperature solders for sustainable replacements of lead-based solders and high-temperature lead-free solders. Compared to solid-state sintering and lead-free solders, TLPS uses lower temperatures and is, thus, suitable for assembling temperature-sensitive components. TLPS is a non-equilibrium process and determining the kinetics is critical to the estimation of processing times needed for good joining. The tin-indium (Sn-In) system with a eutectic temperature of 119°C is being considered as the basis for a TLPS system when combined with tin. Most models of TLPS include interdiffusion, dissolution, isothermal solidification, and homogenization and are based on simple binary alloys without intermediate phases. The Sn-In system has two intermediate phases and thus the reaction kinetics require additional terms in the modeling. Differential Scanning Calorimetry (DSC) has been used to measure the response of Sn-In alloys during the transient liquid phase reaction. Preparation of tin indium alloys for microstructural analysis is challenging due to their very low hardness. This study uses freeze-fracturing of the tin indium alloys to obtain sections for microstructural analysis. The combination of DSC and microstructure analysis provides information on the reaction kinetics. It was observed that the solid/liquid reaction does not proceed as quickly as desired, that is, substantial liquid remains after annealing even though the overall composition is in the single-phase region in the phase diagram.

1. INTRODUCTION

A new generation of low temperature solder technology is required for advanced microelectronic packaging. There is a need to lower the processing temperature to minimize warpage and for the use of temperature sensitive components. However, the required processing temperatures are close to the component use temperatures. Also, increased density requires stacked dies and multiple processing steps. The aim in this work is to create a solder technology that is formed at low temperatures (~130°C), and post processing will be stable to higher temperatures (~200°C). The technology is based on transient liquid phase sintering (TLPS).

1.1 TLPS Applications

Power electronics and microelectronic devices have advanced rapidly and will continue to demand innovative joining technologies as miniaturization continues. There is also a drive to reduce latency without sacrificing computing performance or efficiency. A pragmatic architectural approach has been to reduce the distance from the CPU to memory using packaging technology such as solder interconnects or increase transistor density via vertical stacking of integrated circuits (ICs). Low-temperature TLPS is a technology that may support emerging technologies, namely three-dimensional stacked integrated circuits (3DIC)s and thermal interphase materials [1],[2].

3DICs have increased transistor density, low cost, lower processing temperature, and lower energy per bit consumption in comparison to other IC technologies like 2D/2.5D ICs. Currently, the diameter of the TLPS joints is about 10-20 μm, which is much smaller than ball-grid- arrays[3]. 3DICS may require layering of heterogenous ICs with potentially differing heat tolerances. TLPS uses lower temperatures and is, thus, suitable for assembling temperature-sensitive component

New layers (Figure 1) must be added without impacting the integrity of the previously established layers [1]. Unfortunately, 3DICs suffer from poor thermal management [1]. TLPS solder joints are known to function at higher temperatures than that which they were processed (i.e. 130°C processing temp vs 200°C melting temperature). Creating ultra-low temperature TLPS solder using tin and indium is promising. Tin-indium alloys have a low binary eutectic temperature and large IMC widths for the tuning of solder alloys properties. Sn-In composition is 48Sn-52In with a melting temperature of 119°C. The melting temperature of Sn-Bi and Sn-Pb is 139°C and 183°C, respectively (Table 1).

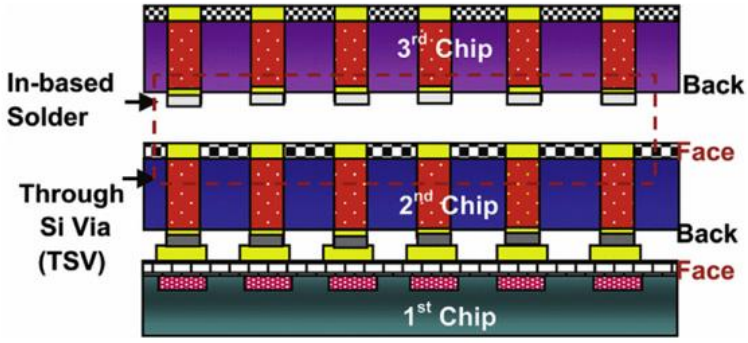

Figure 1 Schematic of a stacked dice fabricated using TLPS [3]

Table 1 Binary Alloys Eutectic Temperatures

Binary Alloys	Eutectic Temperature
Tin + Lead	183°C
Tin + Bismuth	139°C
Tin + Indium	**119°C**

In principial creating low temperature alloys using Sn-In is possible, however, there is a gap in literature detailing the microstructural evolution and the kinetics relating to forming the intermetallic $InSn_4$. The study presented has been conducted to understand how kinetics vary with temperature, isotherm hold time at the maximum temperature and composition.

1.2 Sintering Process

Sintering is a processing method that aims to produce dense compacts (reduce void fraction) via thermal treatment. Sintering can also be used as a joining technology to connect similar and dissimilar materials to one another. Formulation of sintered joints require proper material selection and application of appropriate adjoining techniques. Sintering can be separated into two core processes, solid phase sintering and liquid phase sintering [4]. This work focuses on transient liquid phase sintering (TLPS), which is classified as a liquid phase sintering (LPS) technique.

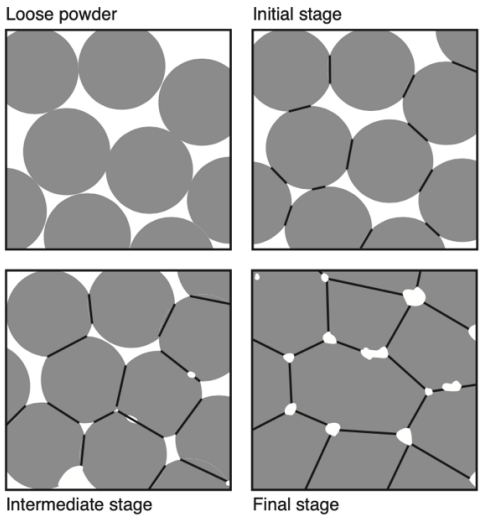

Figure 2 Theoretical Solid Phase Sintering Stages [5]

1.2.1 Solid Phase Sintering

Solid phase sintering (SPS) involves the densification and bonding of solids by heat-treating them below their melting temperature [6]. SPS's driving force is capillary pressure due to introduced heat or pressure. The powder system's attempt to minimizes energy causes neck formation which can lead to densification and/or coarsening/grain growth depending on the kinetics of the different mechanisms[6], [7]. Starting from a green body (Figure 2 (a)), particles undergo three stages. The initial stage (Figure 2(b)) involves interparticle formation of necks and reorganization of grain boundaries. The intermediate stage (Figure 2(c)) promotes further densification and/or coarsening by neck growth, grain growth, and isolation of pores. Finally, the compact eliminates pores via grain boundary diffusion (Figure 2(d)) [7]. The elimination of isolated pores in the final stage takes up most of the process's time[8]. The major contributors of densification are grain-boundary diffusion, lattice diffusion, and plastic deformation to the neck surface [7].

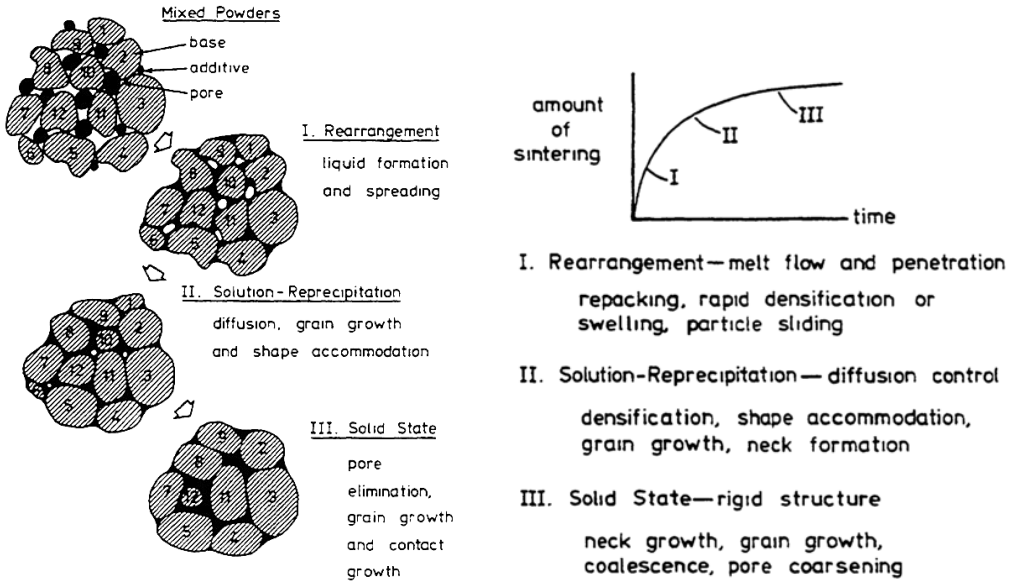

Figure 3 Theoretical Stages of Liquid Phase Sintering and Sintered Time Profile [4]

1.2.2 Liquid Phase Sintering

Liquid phase sintering (LPS) is often used for materials that are challenging to sinter via SPS. A liquid medium provides faster atomic diffusion and better rearrangement than SPS, while not requiring external pressure to densify compacts. Liquid phase sintering (LPS) begins with two kinds of solids particles, one of a lower temperature phase (LTP) known as the additive material (Figure 3), and a high temperature phase (HTP) referred to as the base material [8]. The former melts and spreads quickly during the early stage of sintering while the latter does not melt but partially dissolves into the liquid.

According to classical LPS theory, LPS has three competing stages (Figure 3) of: rearrangement, solution reprecipitation, and solid state diffusion [4]. In Stage I the kinetics associated with rearrangement surpasses other events. The wetting (LTP) liquid, quickly dissolves possible solid-solids necks and applies internal forces on the HTP base via capillary attraction causing rapid

densification in the compact[4]. In Stage II (Figure 3) diffusion and grain growth dominate since the prior dissolution of base material results in a more viscous slower flowing liquid. However, metal melts generally do not have high viscosity. Lastly, stage III involves the reduction of pores via coarsening. The result of classical LPS is a sintered composite material with overall ductile properties, regardless of the quantity of HTP material[9]. Classical LPS suggests that the LTP has solubility in the HTP. Solubility is emphasized because it affects whether the liquid will be persistent or transient.

1.2.2 Transient Liquid Phase Mechanism

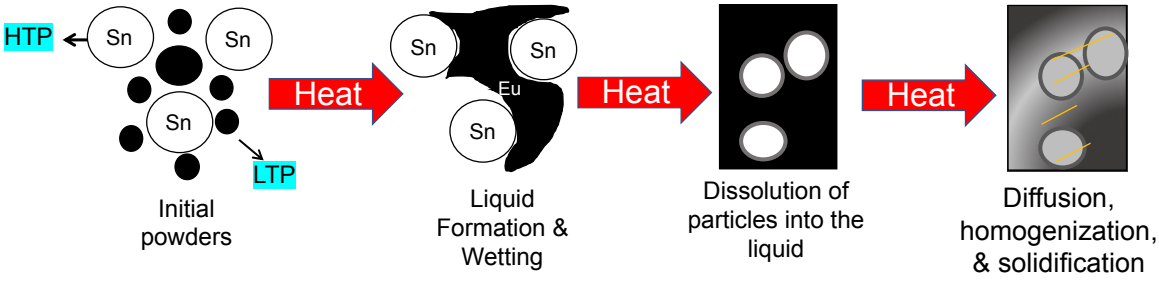

Figure 4 Mechanism of Transient Liquid Phase Sintering (TLPS)

Transient liquid phase sintering (TLPS) is a form a LPS that is used industrially for high and low temperature applications. TLPS can be described as diffusion controlled growth of a new phase involving the dissolution of another phase [10]. During TLPS a thin liquid forms, wets and dissolves the contacting particles, solidifies isothermally, and then homogenizes (Figure 4)[10]. For binary systems the liquid layer is often a LTP eutectic mixture or thin pure foil. Like LPS,

during TLPS a HTP material and a LTP material are in contact and form a liquid by reaction with parent metals (HTP). Unlike LPS, in TLPS the liquid does not persist.

1.3 Challenges With TLPS

Successful formation of TLPS solder requires controlling the transience of the liquid to meet densification criteria. This is a combination of kinetics parameters, thermodynamics, and cost of production and processing [17]. If TLPS is not achieved voids may form and lead to brittleness. IMCs are generally not as dense as their parent metals; IMC joints may not be able to compensate for flaws via plastic deformation like their pure metals do [9]. TLPS solders suffer from the following main challenges. (1) Weak reactivity and slow diffusion between the solute metal and the parent metal can stem from large differences in melting temperatures. Void formation is associated with diffusion couples with drastically differing diffusion coefficients. (2) Materials systems should be isomorphic to reduce complexity, more complex systems may have more phases. (3) IMCs are greatly linked to the thickness and the reactive paths available during formation and relaxation. (4) Another dilemma with the application of TLPS is the miniaturization of joints; micro joints are more challenging to manufacture and run the risk of metastable IMCs induced by aging or harsh environments [17]. Overall, defective joints will limit expected performance and longevity.

1.4 Objective

Research has been conducted using tin-indium paste for applications at low temperatures. Working with solder paste instead of layered systems is advantageous because it allows accurate bulk stoichiometry and reduces the time of solidification because of increased surface area.

The objective of this investigation is to:

- Observe the microstructural evolution and morphology of the solder alloys
- Understand the mechanisms of TLPS in Sn-In by using multidimensional kinetics and thermal models
- Examine the thermodynamic and kinetics behavior of Sn-In using DSC
- Create pathways for empirical models between processing parameters and densification

2. TLPS

2.1 TLPS Background

Multiple forms of research in metal systems have influenced the current model of TLPS. Originally, Duvall et al. investigated TLPS of Ni-Cr-Co (HTP) with Ni-B (LTP) as the filler metal, and suggested TLPS be divided into three stages: base metal dissolution, isothermal solidification of the liquid phase, and joint homogenization. Tuah-Poku et al. examined the bonding of silver (HTP) using copper (LTP) and recommended differentiating the melting of the filler metal from the widening of the liquid region at the bonding temperature [10]. An additional fifth stage of TLPS, based on interdiffusion is suggested by MacDonald and Eager. This is based on their evaluation of Niemann and Garret's research focused on bonding Al-B composite (HTP) using copper (LTP). Macdonald and Eager suggest using low heating rates from room temperature to the eutectic temperature of constituents results in liquid deficiency. Rather than the promotion of bonding via wetting, there is the diffusion of copper from the interlayer into the base [10].

Classical models have certain limitations. Firstly, the model can only be applied with confidence to eutectic fillers or pure elements[10]. Secondly, the model assumes complete wetting of the substrate. Lastly, the heating rate between the eutectic temperature and bonding temperate has a significant impact on the process's kinetics. Insufficient thermal contact alters the traditional four steps of TLPS [10].

2.2 Modelling vs Analytical approaches of TLPS

Previous studies have not extensively studied the impact scaling has on solder joints. Smaller-scale application of solder requires more exactness in experimental designs and analysis. It is tempting

to follow conventional theories used for brazing couples since they follow the same physics (stages). Nonetheless, materials (flux, binder, particle size, and texture), the form of the reacting material (paste, powder, foils), and scale of application that are no considered in the models have important effects.

There are many different variables that affect TLPS. Firstly, considering the material system processing (1) phase diagram assessments(2) diffusion and inter-diffusion coefficients, (3) grain size[11], (4) and particle size. The phase equilibria are determined by the bulk composition, and for transient cases the microstructure of the parent metal and the chemical composition of the filler metal are integral [12]. On the experimental front, parameters such as bonding pressure, bonding temperature, heating rate, cooling rate, and isothermal hold time play a significant role. Zhou et al. developed analytical and numerical models for estimating TLPS. The analytical models rely on approximation solutions such as the error function solution, and parabolic law assumption that treat each stage as a discretized function.

Conversely, the numerical approach is able to estimate the four stages of TLPS simultaneous and more accurately, however, it is very complex and involves predictive estimations[10]. Both analytical and numerical methods assume local equilibrium at the migrating interface, however, local equilibrium is not necessarily attained for the solid/liquid interface during sintering so the approximation lacks precision [10]. The development of a moving boundary necessitates additional constraints at the interface that is unaccounted for when assuming a sharp interfacial boundary. Furthermore, both models assume complete wetting of the base metal for their

estimation [10]. Validating theoretical prediction via experiments have has been troublesome because of the large time expenditure and reproducibility challenges.

2.3 Previous Literature on Quantifying Sintered Metals

Previous studies focusing on validating empirical to theoretical models have done so by running series of multiple experiments, arising from a lack of practical in-situ methods. For instance, Arafin et al. (2007) attempted to bridge the gap between models and experiments by running experiments of wedge type TLPS in conjunction with a diffusion-based model comparison and experienced difficulties[12].

Measuring the transience of the liquid is done by comparing the change in its width versus braze time. This entails applying different hold times at a set bonding temperature (brazing temperature). Afterward, the sample is cooled to room temperature, followed by measuring the width of the centerline solidified liquid region metallographically [12]. This approach assumes that the liquid width at the bonding temperature remains the same when cooled to room temperature. To curtail error, multiple runs with ample range of hold times are necessary. This will cost additional time and resources. Additionally, the analytical solution assumes that the interface is planar, when in fact the interface is likely to be scalloped.

Corbin and McIsaac were the first to successfully model and quantify the stages of TLPS using DSC in powder mixtures. Corbin and McIsaac quantified the amount of initial liquid formed in the TLPS bond as well as the amount found during the duration of the sintering process [13]. Two isomorphous systems (Ni-Cu, Sb-Bi), two eutectic systems (Pb-Sn and Sn-Bi), and two alloys with two or more intermediate compounds (Cu-Sn and Sb-Sn) were considered in their work.

Kuntz et al. published a technique based on DSC that could measure the liquid fraction present during TLPS for a simple Ag-Cu binary system with slow diffusing Cu as the LTP material. They were able to quantify the magnitude of the eutectic-solidification-enthalpy during the cooling of a TLPS joint by interrupting experiments before complete solidification occurred[12]. Within sixteen experiments, Kuntz et al. were able to determine the rate of isothermal solidification and the total isothermal time, by running replicates in succession with time evolution ranging from 1 minute to 14. Microstructural measurements were made in tandem using the centerline eutectic width to validate DSC enthalpy measurements[12].

Corban and McIsaac's research stated that the first stage of TLPS is solid-phase interdiffusion (similar to MacDonald and Eager), followed by melting and dissolution, liquid spreading and re-solidification, and lastly secondary solidification. Using different mediums (powders with flux vs. drying milled powder with no flux) registered distinct signatures with DSC For the Sb-Bi system, a sharper endotherm peak was associated with powders without flux, and a broader, smaller endotherm was witnessed in powders containing flux. Corban et al. suggest that surface oxides can create barriers that precluded solid-phase-interdiffusion at the early stages of melting and dissolution [13]. The reduction of an oxide barrier via flux changes the melting behavior and correlate to reduction in the melting endotherm [13]. In other words, the observed interdiffusion of Sb and Bi is due to unlimited solubility in solid-state diffusion, or a reduction in the energy barrier needed to nucleate a new phase[13]. Corbin and McIsaac's research also emphasized that DSC was capable of quantifying the effect of size and grain structure. Their experiments matched predictive modeled trends for Eutectic Sn-Pb.

2.4 Tracing Transience using DSC to measure Remaining liquid fraction

DSC measures the heat flow into or out of the sample (calorimeter) against that of a reference (differential) during a constant or dynamic thermal cycle (scanning). DSC has the ability to quantify physical and chemical changes in real-time for a given TLPB system. It also provides insight into the kinetics of isothermal solidification [13]. Typical metallographic methods involve surveying isolated cross-sections; cross-sections are useful but unable to definitively quantify the solid\liquid interactions in TLPB without extrapolation. Using a cross-section for empirical research inherently limits the sample size of a given data set, which in turn forces models to use approximations as compensative means.

Many researchers like Kuntz, Mullins, McIsaac, Corbin et al., and Ikeuchi et al. have pointed out that analytical models developed from relying on isothermal solidification can be inaccurate, and that error increases as the material systems complicates (i.e., polycrystallinity, and multiphase alloys systems). DSC's advantage is that it provides real-time quantification of the liquid fraction within a TLPB. However, even though DSC is powerful, it still may require microscopy to corroborate findings, especially when the signatures are convoluted or indeterminate [14].

With a DSC trace it is possible to calculate the liquid to solid volume ratio for an alloy sample. Integrating the endotherm marks the heating event and integrating the exotherm marks the cooling events. Dividing the area of the endotherm to the exotherm yields the liquid to volume fraction. The melting of the sample is characteristic of the endotherm peak and the solidification is that of the exotherm peak. For pure metallic sample and eutectic samples, the solidification exotherm ΔH_s divided by the melting endotherm ΔH_f should be very close to unity. For a binary material (alloy)

with different phases of differing melting temperatures, annealing for different length can determine the level of diffusion or reaction occurring[13], [14]. It is possible to have slight variations amongst the different alloys. Variation may be due to possible loss of small amounts of mass (vapor, flux, etc.) that may be corrected for by normalizing with the change in mass. Additionally, probe sensitivity and sample size are parameters that may impact the overall variation. When using the comparison of the ratio to understand diffusion in alloys, it is important to establish a consistent measure to avoid bias.

$$\%\text{Liquid Fraction} = 100 \times \left(\frac{\Delta H_s}{\Delta H_f}\right) \text{ Eqn. 1}$$

2.5 Equations of Diffusion: Isothermal kinetics of reaction and diffusion in a simplified Sn-In

Factors that impact the reaction and diffusion of alloys in a TLPS system generally are the heating rate, anneal time, anneal temperature, particle size and the concentration of the solute. The experiments performed in this study are with powders which differs from literature on planar systems for transient liquid phase sintering. To leverage previous analytical solutions powders are assumed to similar in size and spherical[10].

Fick's first law can be used to represent the mass flux (J) of the diffusing LTP eutectic solute atoms[10], [14].

$$J = -D \cdot \left(\frac{\partial C}{\partial x}\right) \text{ Eqn. 2}$$

Fick's second law is invoked for non-steady diffusion where the concertation changes as a function of position and time. Certain assumption must be made to use Fick's first and second law

analytically, in the 1-D case, local equilibrium at the solid/liquid interface is required, there must be no concentration gradients in the liquid, constant diffusion *D* is assumed *, and* a semi-infinite solid media is assumed[10], [14]. In the case of our alloys, the HTP Sn matrix can contain all of the diffusing solute. Resultantly, during the dissolution stage the growth process can be estimated using the square root law[15] [16].

$$\frac{\partial C}{\partial t} = D \cdot \left(\frac{\partial^2 C}{\partial x^2}\right) \text{ Eqn. 3}$$

The solid/liquid interface interaction is expressed as a mass balance equation:

$$(C_L - C_S)\frac{d}{dt}X(t) = D_S\frac{\partial}{\partial x}C_S - D_L\frac{\partial}{\partial x}C_L \text{ Eqn. 4}$$

Where x= *X*(t) represent the position of the interface as a function of time, C_L and C_S represent the concentration of liquid and solid at the interface at the solid/liquid interfaces, and D_S and D_L are the diffusivities [14].

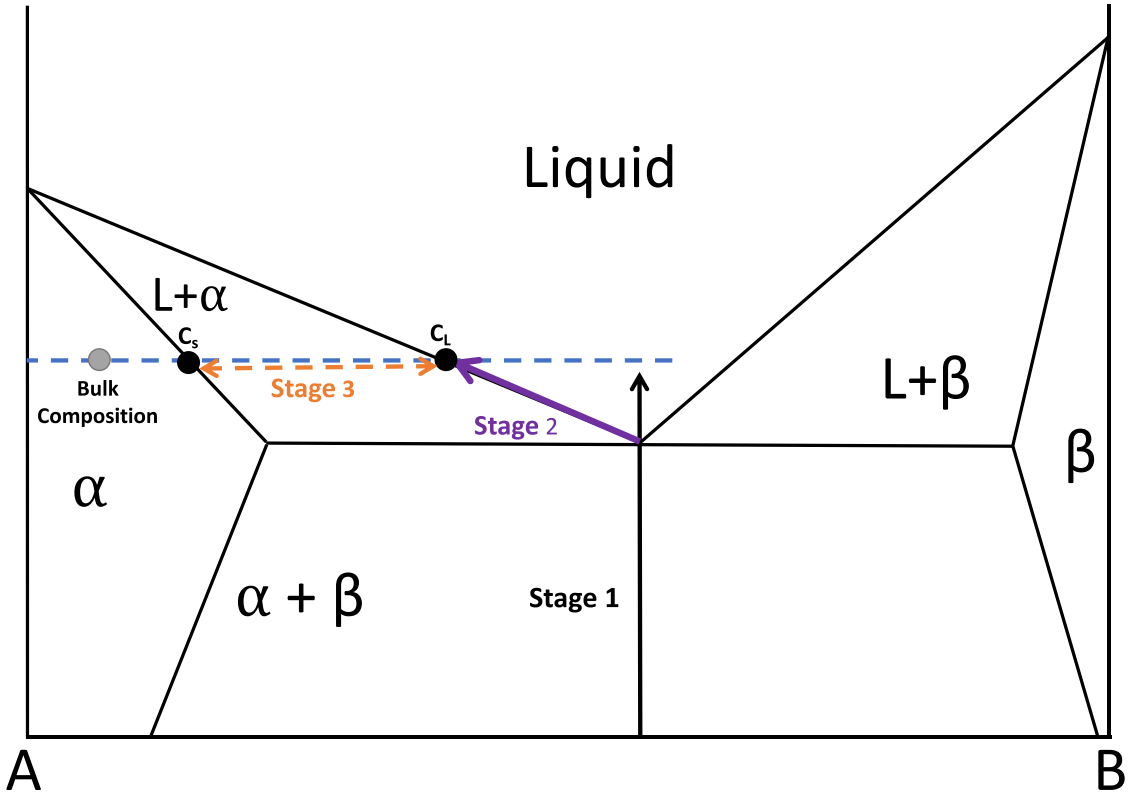

Figure 5 A schematic of a binary phase diagram at a processing temperature indicated by the blue dotted line.

Consider the simplified binary phase diagram containing no intermediate phases (Figure 5). For the TLPS reaction, select an alloy with an overall composition in the single phase at the isothermal hold temperature (α−phase in gray). Next isothermally heat the alloys above the eutectic temperature and allow the diffusional transformation to occur. Stage 1 is the heating stage where the liquid forms when it passes the eutectic temperature. Stage 2 represent the rapid dissolution of Sn particles into the eutectic liquid. Stage 3 is the isothermal solidification and is slower than the previous 2 stages. Lastly, Stage four represent the homogenization step or an equilibrium phase when the bulk concentration has reacted sufficiently.

For a processing temperature indicated in Figure 5 during isothermal solidification the interface composition will be bounded by a tie line between points Cs and C_L. The diffusion of the liquid solute into the HTP material can be modeled with the semi-infinite approximation. The motion of the solute into the solid phase will result in a solid/liquid moving boundary that forms more solid phase by epitaxial growth until the liquid is consumed [14]. The aforementioned conditions allow for the simplification of boundary conditions:

Initiation Conditions	$C(x,0) = C_O$	
Boundary Conditions	$C(0,t) = C_S$	$C(\infty,t) = C_O$

Using the analytical discretized model, Co and Cs are the initial values of the solute and solid, respectively at the processing temperature. Time zero marks the beginning of the isothermal solidification (stage 3). Time zero also infers that the dissolution stage happens orders of magnitude faster than the isothermal stage, so artifacts of the dissolution stage can be ignored. Assuming local equilibrium prior to isothermal dissolution justifies the first boundary condition

when x=0 at the solid/liquid interface. At the interface for x>0 the tie line predicts the solidus and liquidus concertation will be constant while holding the processing temperature. The next boundary condition x=∞, via the semi-infinite approximation suggests that far away from the interface concentration does not impact the base material matrix (Sn).

An analytical solution to the isothermal stage can be adapted from Crank:

$$C(x,t) = C_S + (C_O - C_s) \cdot erf\left(\frac{x}{2\sqrt{Dt}}\right) \text{ Eqn. 5}$$

Assuming a constant diffusion coefficient, boundary conditions, and applying approximations creates further insight into what occurs during the isothermal stage.

2.6 Equations of Diffusion: Reaction and diffusion in a binary phase diagram

Previous solutions for estimating the duration of the isothermal phase have been attempted by Tuah-Poku and McDonald. These models often had issues with estimating the completion time because they assume a stationary interface. The older models, however, hold true in instances where the k (the reaction rate) value is small.

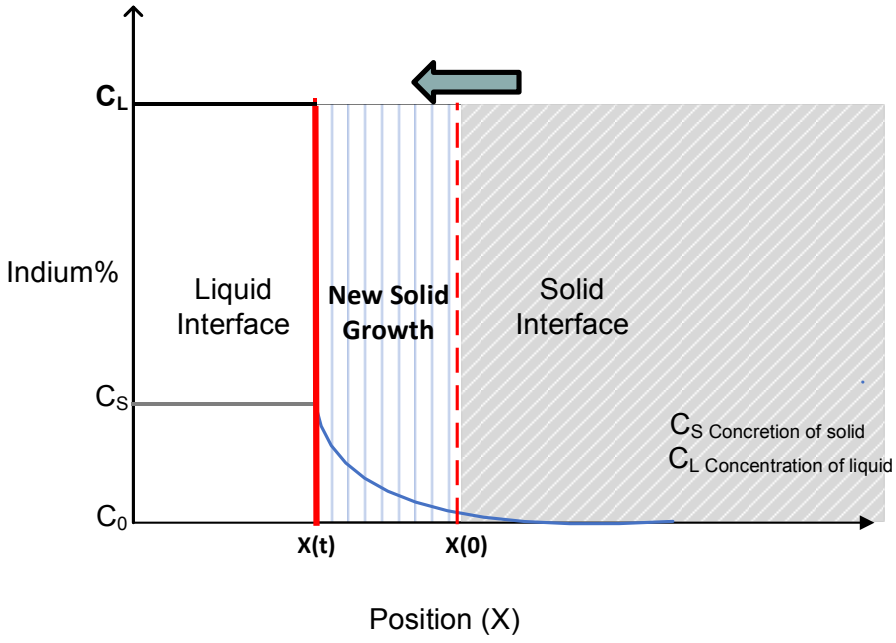

Figure 6 Schematic for the moving solid/liquid interface phase boundary. The red dash indicates the starting solid/liquid interface and the solid red line represent the new solid/liquid as isothermal solidification takes place.

When a solder paste is sintered at a constant temperature, there will be a net flux stemming from a concentration gradient or chemical potential differences. For transient liquid phase bonding, the sites of solid and liquid interfaces will have a moving boundary as the liquid solute penetrates the solid tin matrix as seen in Figure 6 above. At the solid/liquid interface as time elapses, more new solid growth occurs as a result of the difference in concentration and chemical potential between the solute (indium rich liquid) and the solid tin interface. At t=0 the dash red line represents the solid/liquid interface and X(0) is the solute concentration of the solid. The solid red line represents the solid/liquid interface after some time. The new growth and progression of time will result in a migrating solid/liquid interface. The differentiation between LPS and TLPS was made earlier. As

long as the liquid does not persist, the growth of the new phase can be analytically solved as a moving boundary.

Lesoult et al. proposed a more thorough approach to the error function solution.

$$C(x,t) = A_1 + A_2 \cdot erf\left(\frac{x}{2\sqrt{Dt}}\right) \text{ Eqn. 6}$$

Where A_1 and A_2 are constants predetermined by boundary conditions invoked.

Applying previous boundary conditions very far away from the interface:

Where $x \rightarrow \infty$,

$$C(\infty,t) = A_1 + A_2 = C_0 \quad \text{Eqn. 7}$$

Applying previous boundary at the moving solid/liquid interface

Where $x \rightarrow X(t)$,

$$C(\mathrm{x(t)},t) = A_1 + A_2 \cdot erf\left(\frac{X(t)}{2\sqrt{Dt}}\right) = C_S \quad \text{Eqn. 8}$$

It's more relevant to focus on solving the solid/liquid interface as a migrating boundary value problem verses a static boundary problem. Although a discretized analytical model makes many different assumptions and potential omissions, such a model that estimates the reaction rate. For the solid/liquid interface that forms, the analytical solution can estimate the rate by which the liquid (solute) is consumed. Accounting for the shrinking liquid interface in TLPS can be done by defining a reaction rate that is proportional to the change in the interface. The k value is similar to a first order rate law.

A large k value indicates a shorter isothermal solidification with rapid solid/liquid interfacial movement [17]:

$$k = \frac{x(t)}{2\sqrt{Dt}}$$ Eqn. 9

The value of k can be substituted back into the analytical solution. Rearranging the value to solve for x(t), the relationship between the reaction rate of the solid and the time required for diffusion becomes clearer:

$$x(t) = k2\sqrt{Dt}$$

The square root law approximation can only be used for the third stage of TLPS isothermal solidification, since the dissolution stage (stage 2) is assumed to occur very rapidly in alloys processed in paste mediums. Equation 5's constant can be re-written as a function of k.

$$A_1 = C_o - \frac{C_s - C_o}{\mathrm{erf}(k) - 1}$$ Eqn. 10

$$A_2 = \frac{C_s - C_o}{\mathrm{erf}(k) - 1}$$ Eqn. 11

$$C(x,t) = C_o - \frac{C_s - C_o}{\mathrm{erf}(k) - 1} + \frac{C_s - C_o}{\mathrm{erf}(k) - 1} \cdot erf\left(\frac{x}{2\sqrt{Dt}}\right)$$ Eqn. 12

Further simplification can be done to create a graphical solution by considering non-dimensional mass transfer coefficient, however, doing so adapts a solution without geometric consideration and will ultimately require a correction factor[15].

3. TLPS FOR SN-IN ALLOY

3.1 Tim and Indium Properties

Table 2 Tin Indium Properties [18] [19]

Property	**β-Tin**	**Indium**
Crystal Structure	BCT	BCT
Van der Waals radius (pm)	217	193
Empirical Atomic Radius (pm)	140	167
Density (25C) g/cm^3	7.265	7.31
Molecular Weight	118.7	114.8
Atomic number	50	49
Thermal Property		
Melting temperature °C	232	156.6
CTE (at 25°C) μm/(m·K)	22.0	32.1
Heat of fusion (kJ/mol)	7.03	3.281
Mechanical Properties		
Mohs Hardness	1.5	1.2
Poisson's Ratio	0.33	0.45

TLPS for semiconductor or electronic application requires good conduction, thermal resilience, and mechanical properties. Similarities between tin and indium can be seen in Table 2 above. Compared to other available low-temperature metals such as lead, or thallium, indium is much less severe in toxicity. In addition to the aforementioned properties, it has a very low eutectic temperature compared to other lead-free alloys.

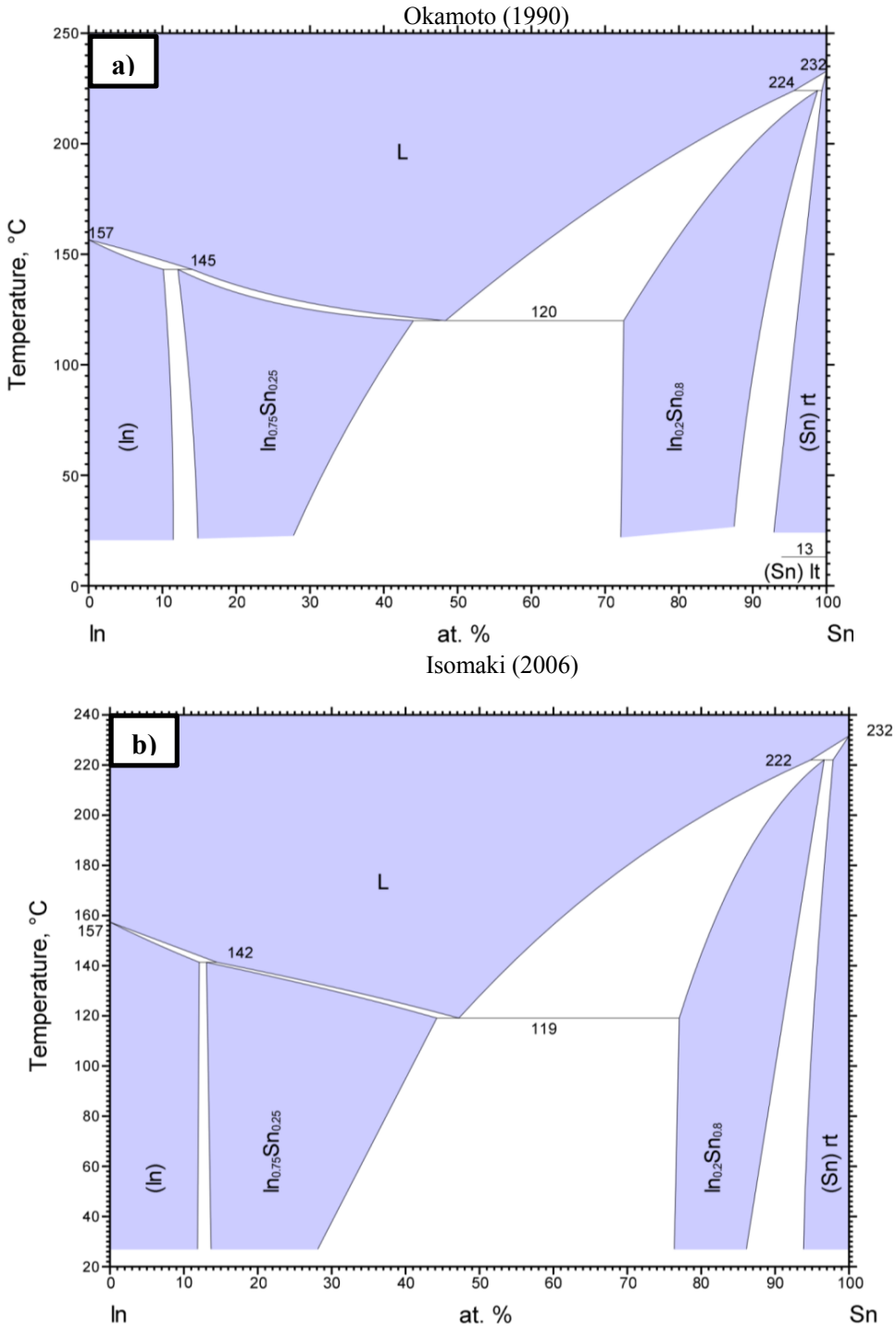

Figure 7 Tin-Indium phase diagrams (a) Okamoto an experimental phase diagram (b) Isomaki a computed phase diagram [20], [21]

3.2 Phase Diagrams

Previously a binary phase diagram was used in figure 5 to describe the stages of TLPS. A variety of tin indium phase diagrams are published. The ASM Alloy Phase Diagram Database records 14 different versions at the moment. More recent Sn-In phase diagram agree on the eutectic temperature and the eutectic composition however their phase boundaries vary (Figure 7). The Sn-In binary system is more complex than other simple binaries such as Sn-Pb or Sn-Bi because it contains two intermediate phases (In_3Sn and $InSn_4$). The two most referenced phase diagrams are the Okamoto et al. phase diagram published in 1990 and the more recent Isomaki phase diagram published in 2006.

There is interest in Sn-In because it has a low eutectic temperature of 119°C at a composition of 48% Sn and 52% In (atomic percent). The melting points for In and Sn are 157°C and 232°C, respectively. Both Sn and In are soluble within each another (Sn into In is 12%, In into β-Sn is 8%). Owing to the expensive cost of pure Indium, TLPS is generally conducted in the Sn rich area of the phase diagram.

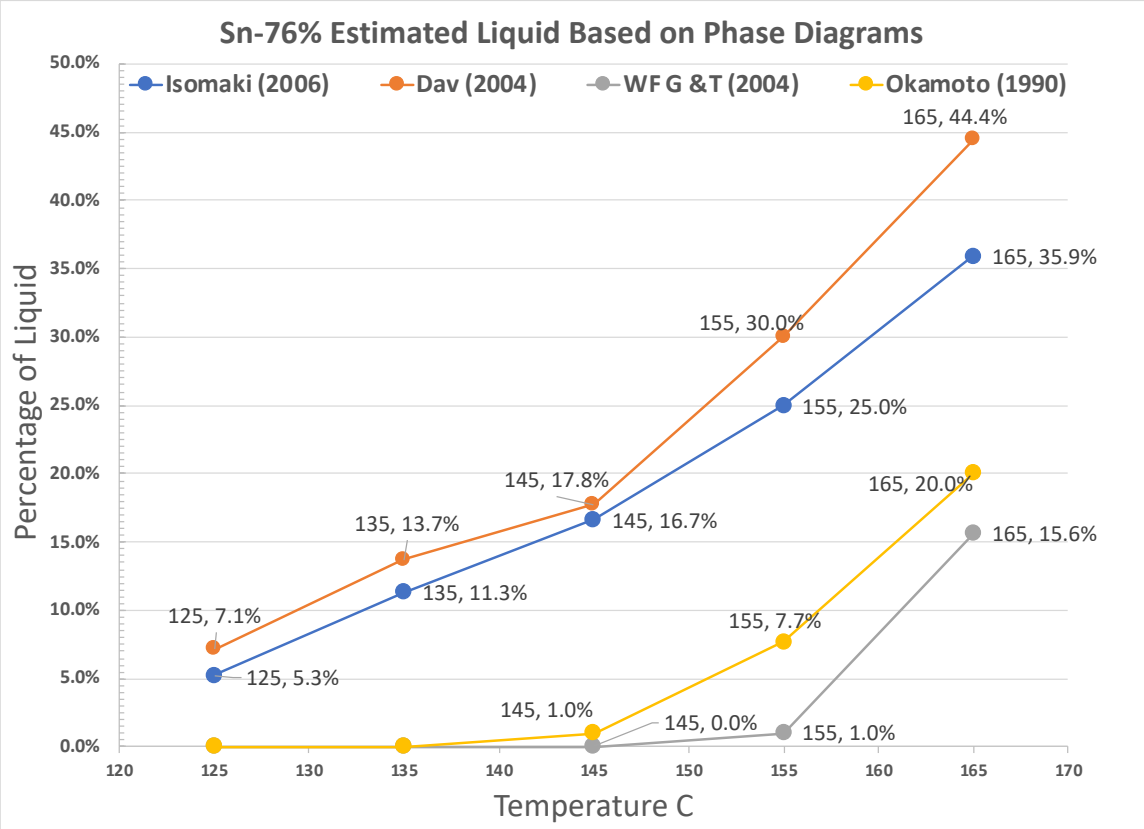

Figure 8 Calculated phase fraction of the liquid from various phase diagrams for the overall composition of Sn-76%In-24%. The Okamoto and W.F. G&T predictions are more conservative than the Isoamki and Dav. [20][21] [22] [23]

Consider the projected $InSn_4$ (C_s) and liquid (C_L) fractions from various phase diagrams in figure 8 above. According to the Isomaki and Dav phase diagram from room temperature until melting an alloy with an overall composition (bulk composition) of 76% Sn would be located in the two-phase region, while according to the phase diagrams published by WF G&T et al. and Okamoto et al. the bulk composition is in the single phase region. At equilibrium Isomaki et. al and Dav et al. predict that the alloy system will have a persistent liquid as seen in LPS. Contrastingly, according to WF G&T and Okamoto et al. the liquid will not be persistent and TLPS is possible. In the case of creating a well densified solder, it is important that there is sufficient liquid in the solder to wet

the tin particles. Poor wetting will result in a solder joints with voids. An idealized table focusing on the Okamoto and Isomaki phase diagram is found in Table 3 below.

Table 3 Expected phases according to the Okamoto & Isomaki Phase Diagrams at 125°C

Diagram	Okamoto	Isomaki
Sn%	Phases	Phases
74%	1	2
76%	1	Boundary
79%	1	1
82%	1	1
84%	1	1

3.3 The Okamoto and Isomaki Phase Diagram

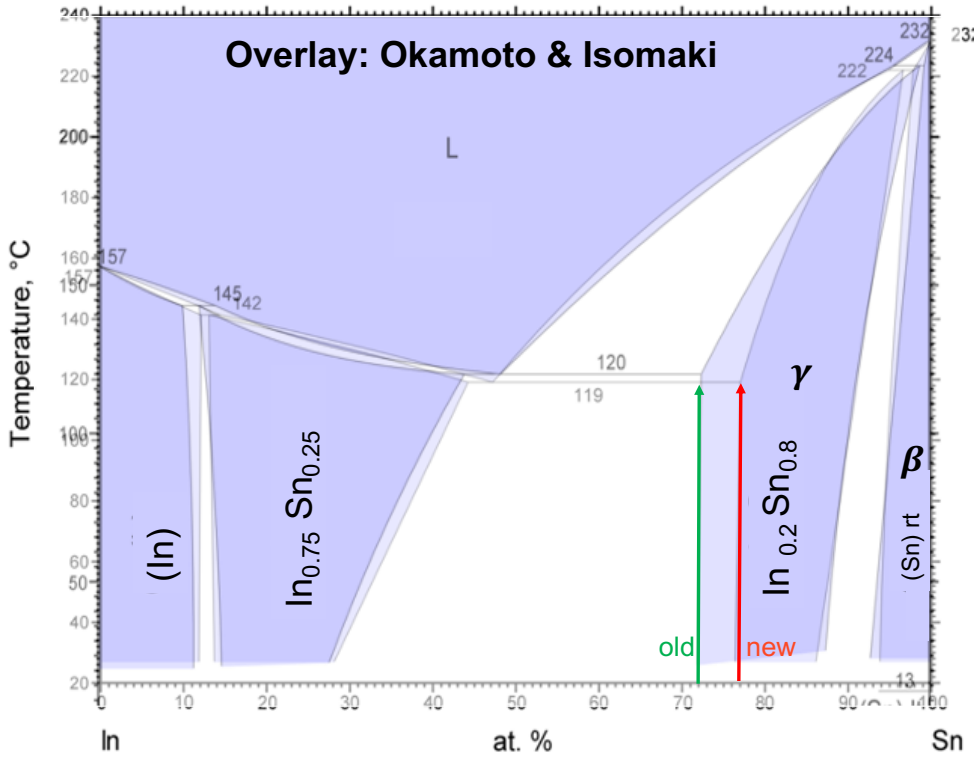

Figure 9 Overlay of the Okamoto and Isomaki phase diagram to emphasize the difference in the $InSn_4$ phase boundary. (not to scale)

The first basic difference between the two-phase diagrams is that the Okamoto is an experimental phase diagram and Isomaki is a computational phase diagram. Isomaki reports a lower $InSn_4$ solubility limit. Super-imposing the former accepted limit reported by Okamoto (1990) over the work of Isomaki (2006) reveals a 4% reduction of the $InSn_4$ solubility concentration for temperature range 20°C to 120°C (Figure 9 old and new boundary). The 4% difference in concentration is important. The overall composition must be in a single-phase region for a TLPS bond to form. This work surveys regions within and adjacent to the phase boundary limits to understand what phase diagram better represents system behavior. The concentrations being studied are from 74% Sn to 84% Sn. A gap in literature exists involving the formation of the gamma phase and difference are reported relating to the solubility limit of $InSn_4$.

Table 4 Phase fraction calculations for the liquid and gamma phase during equilibrium and metastable conditions based on the lever rule

Equilibrium Phase Fraction

125°C Equilibrium Phase Fraction

	76% Sn		79% Sn		84% Sn	
Phase	Liquid	Gamma	Liquid	Gamma	Liquid	Gamma
Okamoto	0.0%	100.0%	0.0%	100.0%	0.0%	100.0%
Isomaki	5.3%	94.7%	0.0%	100.0%	0.0%	100.0%

135°C Equilibrium Phase Fraction

	76% Sn		79% Sn		84% Sn	
Phase	Liquid	Gamma	Liquid	Gamma	Liquid	Gamma
Okamoto	1.0%	99.0%	0.0%	100.0%	0.0%	100.0%
Isomaki	11.3%	88.7%	1.0%	99.0%	0.0%	100.0%

165°C Equilibrium Phase Fraction

	76% Sn		79% Sn		84% Sn	
Phase	Liquid	Gamma	Liquid	Gamma	Liquid	Gamma
Okamoto	35.5%	64.5%	16.1%	83.9%	0.0%	100.0%
Isomaki	35.9%	64.1%	20.5%	79.5%	0.0%	100.0%

Dynamic Phase Fraction

125°C Dynamic Phase Fraction

	76% Sn		79% Sn		84% Sn	
Phase	Liquid	Gamma	Liquid	Gamma	Liquid	Gamma
Okamoto	48.0%	52.0%	42.0%	58.0%	32.0%	68.0%
Isomaki	48.0%	52.0%	42.0%	58.0%	32.0%	68.0%

135°C Dynamic Phase Fraction

	76% Sn		79% Sn		84% Sn	
Phase	Liquid	Gamma	Liquid	Gamma	Liquid	Gamma
Okamoto	52.2%	47.8%	45.7%	54.3%	34.8%	65.2%
Isomaki	52.2%	47.8%	45.7%	54.3%	34.8%	65.2%

165°C Dynamic Phase Fraction

	76% Sn		79% Sn		84% Sn	
Phase	Liquid	Gamma	Liquid	Gamma	Liquid	Gamma
Okamoto	70.6%	29.4%	61.8%	38.2%	47.1%	52.9%
Isomaki	72.7%	27.3%	63.6%	36.4%	48.5%	51.5%

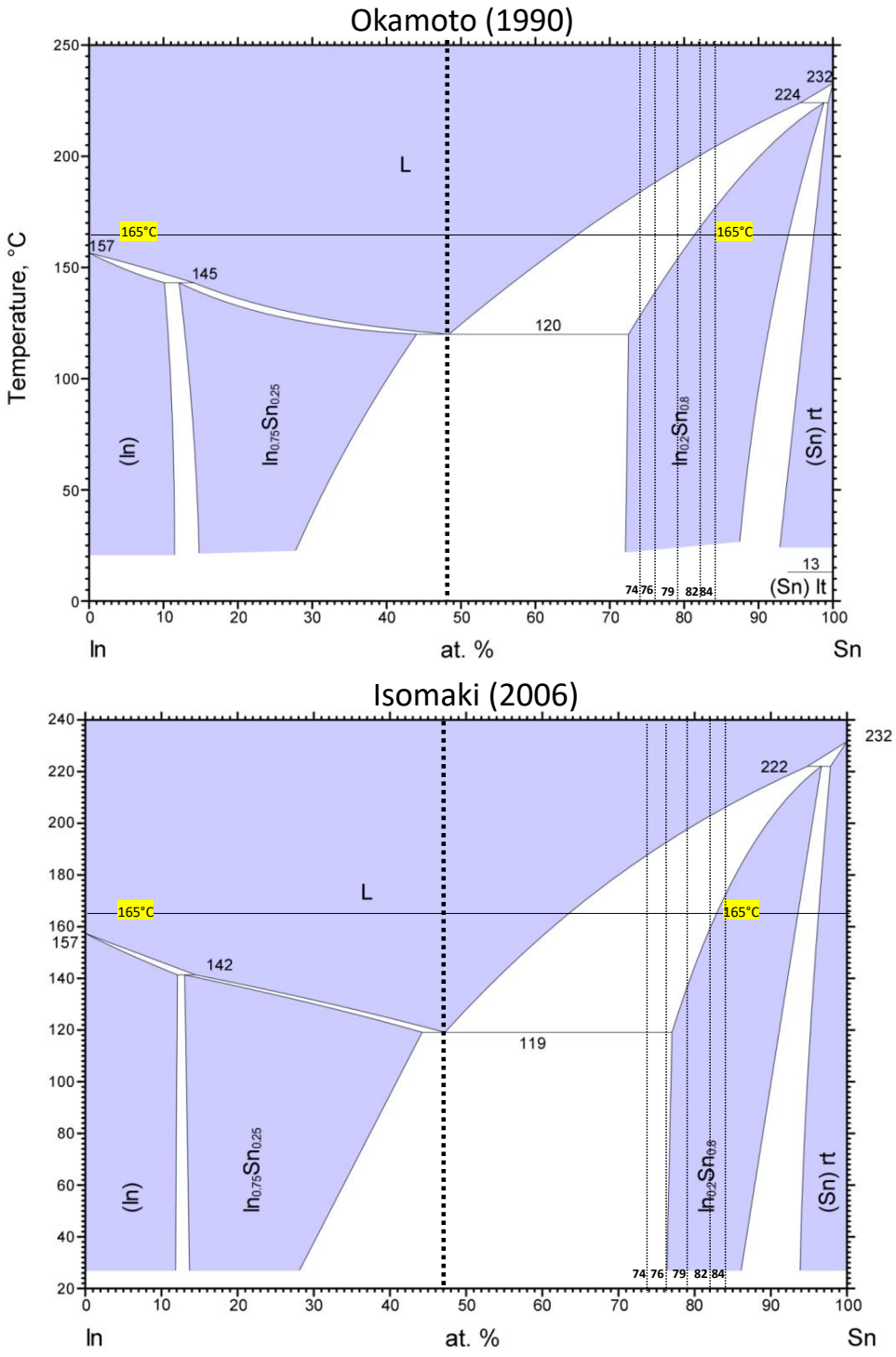

Figure 10 Phase diagrams depicting the difference for compositions at a processing temperature of 165°C. [20], [21]

The equilibrium phase diagram can be used to understand the equilibrium composition of the constituents as well as the metastable projection prior to equilibrium for TLPS system (Figure 10). The metastable phase diagram is derived from applying the lever rule from the liquidus line to a bulk concentration and then extending from the bulk concentration to the pure tin region of the phase diagram. That is, it is initially assumed that at short times the only two phases in the system are pure Sn and liquid of the liquidus composition. Most of alloys have been processed at 125°C – just above the eutectic temperature, at 135°C, and at 165°C. In comparing the Isomaki and Okamoto phase diagrams, there are greater differences between the lever rule calculations of phase fraction for the equilibrium phase diagrams than the dynamic diagram. This is to be expected because the liquidus surfaces for both phase diagrams are similar, while the solidus surfaces for the $InSn_4$ are very different.

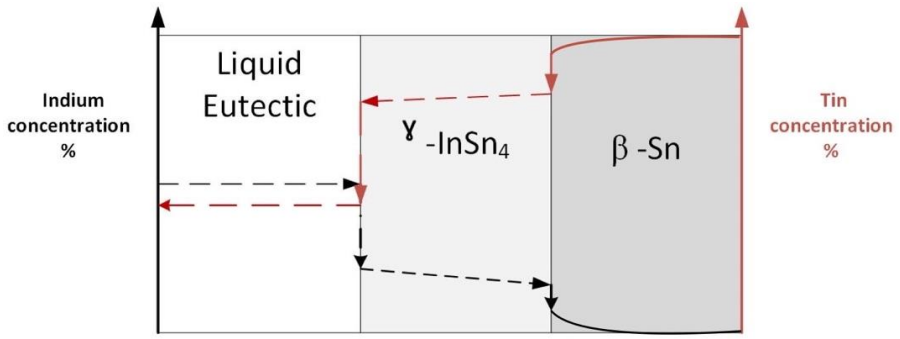

Figure 11 Reaction profile for a finite area of Sn reacted with liquid Sn-In eutectic

3.4 Sn-In Phase transformation

The hypothesis is that reacting the Sn-In eutectic liquid with pure tin for bulk concentrations within a single phase should result in the growth of the $InSn_4$ phase. Keep in mind this is for a reaction occurring where all constituents reacting are not liquified. The $InSn_4$ intermediate phase grows

due to diffusion of solute into the HTP material (Sn) as well as by diffusion from β-Sn (Figure 11). As the eutectic liquid reacts it is also consumed the black arrows signify the change solute concentration. It is also possible for solute to diffuse from the β-Sn to grow the new γ -$InSn_4$ phase. When reacting pure Sn and SnIn-eutectic composition, the SnIn-Eutectic component will be the first to melt. During the initial melting, the amount of liquid is equal to weight fraction of the eutectic. The eutectic liquid wets the tin particles and the liquid fraction increases by dissolving the tin particles. The first question that needs to be considered is where the $InSn_4$ phase grows from if the system is not completely liquified. If the system were completely liquid upon cooling nucleation of the $InSn_4$-gamma phase would be noticed after crossing the liquidus boundary line. However, for a solid/liquid interfacial reaction does $InSn_4$ occur when the liquid is super-saturated from dissolution of tin particles or does the formation of $InSn_4$ only occur when enough solute has penetrated the HTP phase – where diffusion dominates the densification and phase transformation.

Building off the assumption that stage 1 (melting) and stage 2(dissolution) happen rapidly, the growth of IMC phases is more likely to happen during later stages such as isothermal solidification and homogenization. Figure 10 displays the isothermal solidification (stage 3) taking place in the 2 phase region for samples with tin percentage from 74% to 79%. If the sintering process of stage 3 was halted prior to reaching equilibrium and cooled there is a possibility of forming an indium rich IMC ($In_{0.75}Sn_{0.25}$ or In_3Sn) , or a tin rich IMC ($In_{0.2}Sn_{0.8}$ or $InSn_4$). The formation of either intermetallic will heavily rely on the processing temperature and the homogeneity of the LTP eutectic component. The assumption of a well-mixed eutectic solder paste minimizes the chances of the tin rich IMC formation.

The wide concentration width of the intermediate phase found in the $InSn_4$ suggests stability over a range of compositions. The wide concentration gradient may result in differing bulk properties. This also indicates that the intermediate phase has a wide range of metastability. Ordering of the atoms with the alloy can result in Sn-Sn, Sn-In, and In-In type of bonding. As alloys are sintered it's likely that IMCs may form due to short range ordering and affinity.

Table 5 Crystal data for tin indium reported for the Isomaki phase diagram [20]

APD phase label	Formula	Prototype	Pearson symbol, space group	Density (Mg/m^3)	Volume (nm^3)	Cell parameters (nm)	Cell parameters (°)
(In) tetragon	In0.87Sn0.13	In	tI2 I4/mmm	7.81	0.049039	a=0.317 b=0.317 c=0.488 T=298 K	alpha;=90 beta;=90 gamma;=90
In0.75Sn0.25 Tet-alph	In0.75Sn0.25	In	tI2 I4/mmm	7.31	0.05261	a=0.3459 b=0.3459 c=0.4397 T=267 K	alpha;=90 beta;=90 gamma;=90
In0.20Sn0.8 InSn-gam	In0.2Sn0.8	(Hg0.1Sn0.9)	hP1 P6/mmm	7.35	0.02664	a=0.3205 b=0.3205 c=0.2995 T=248 K	alpha;=90 beta;=90 gamma;=120
(Sn) rt BCT_A5	In0.05Sn0.95	Sn	tI4 $I4_1/amd$	7.29	0.10804	a=0.58274 b=0.58274 c=0.31814 T=298 K	alpha;=90 beta;=90 gamma;=90

When considering the reaction pathways of Sn-In to form the gamma (In0.2Sn0.8), there are a variety of ways the reaction may proceed. Three different scenarios will be considered. (1) Firstly, consider the instance of ordering. (2) Secondly, we can consider favorable reaction due to similar crystal BCT structures of Sn and In. (3) Lastly, we can consider the scenario that requires a supersaturation of Sn before the phase transformation. Previous studies by J Morris et al. suggested that the γ phase would resemble a solid solution when constituents were liquified prior to solidification [24]. Discrepancies will arise in this study because the eutectic composition is the primary liquid.

4. EXPERIMENT PLANNING

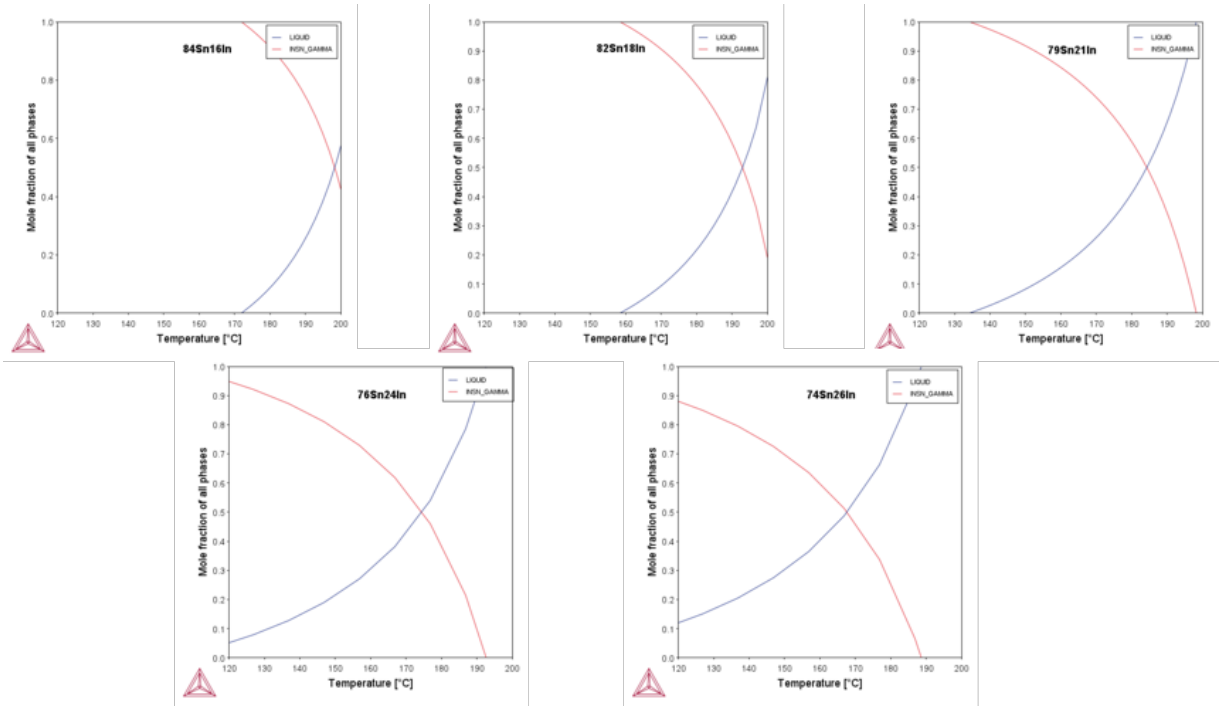

Figure 12 Computational values of the mole fraction of phases depending on the composition from temperature range of 120°C to 200°C

Thermocalc's mole fraction phase predictions were used as a guide for pre-sintering and post-sintering analysis. The default phase diagram used in Thermocalc is that of Isomaki and can be used to confirm the manual equilibrium phase diagram (Table 4) as well as mol fraction of C_s and C_L per bulk concentration. It also expresses the relationship between temperature and phase stability.

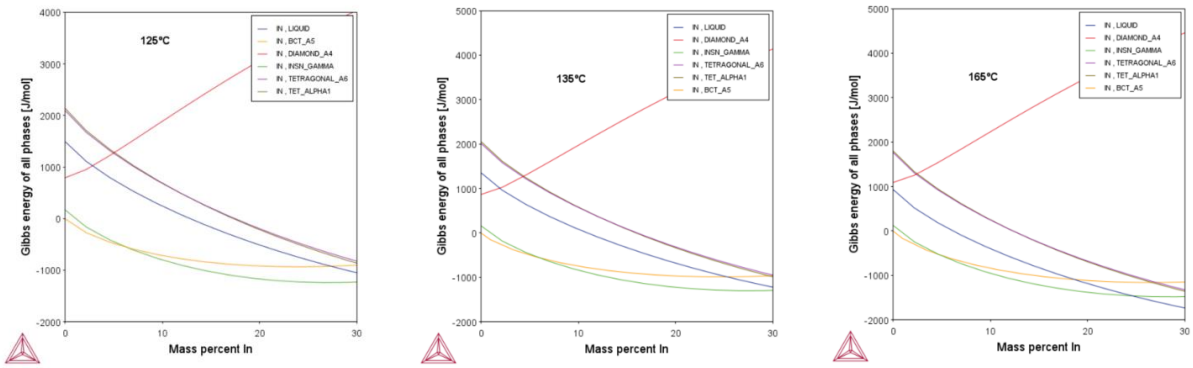

Figure 13 Free energy of curves of phases for (a) 125°C (b) 135°C (c) 165°C based on the Isomaki phase diagram

Thermocalc was also used to understand the stability of phases as a function of the temperature and indium content (Figure 13). A temperature of 125°C slightly above the eutectic temperature, to ensure full melting of the eutectic liquid. The free energy G(T,P) of the system is a function of temperature and pressure. Since the solder will be processed at atmospheric pressure, the temperature has been varied such that phase equilibria varies with differing processing temperatures. Temperatures 135°C and 165°C were selected to distinguish between zones of a persistent liquid and a transient liquid. Higher temperatures were also used to ensure that the reaction proceeded.

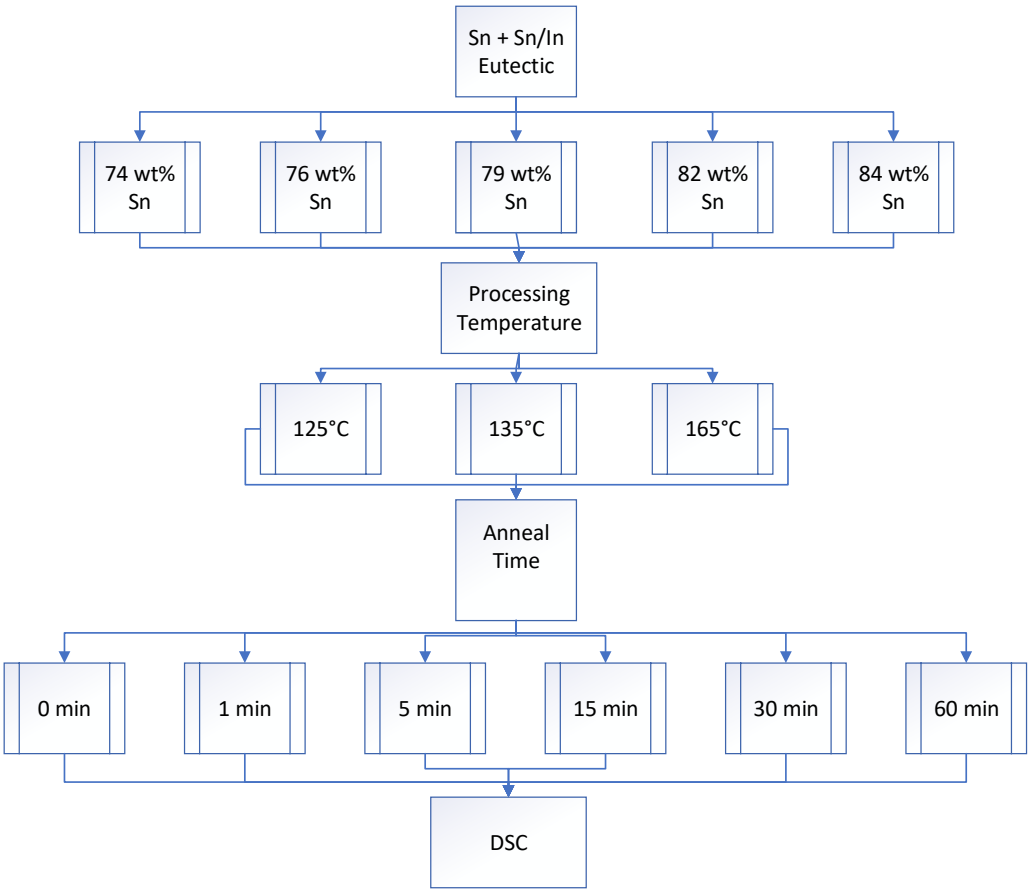

Figure 14 Design of experiment for Sn and Sn-In eutectic that is mixed to form concentrations from 74% to 84% Sn. Afterward the formulated concentrations are annealed using DSC for specific durations. The heating rate is 20 °C/min fand the cooling rate is 10 °C/min.

The design of experiment matrix Figure 14 was created to assess the more accurate phase diagram for TLPS of solder paste and create an empirical method to link processing parameters to the kinetics of the alloys. Tin-Indium eutectic is mixed with high purity tin to create compositions of interest. The response variable for the DOE is the liquid fraction remaining after the sintering of the sample. The controlled variables are the anneal time, temperature, and composition.

4.1 Experimental Methods

Tin-Indium alloys comprised of eutectic solder paste and tin solder paste were used to investigate the evolution of TLPS. Commercial Sn-In eutectic solder paste consisting of 52In/48Sn was purchased from Indium Corporation. Sn-0.7Cu-0.05Ni was provided by Nihon-Superior Co. Japan. Formulated alloys had compositions ranging from 74% to 84% of Sn. Stoichiometries of 74%, 76%, 79%,82%, and 84% were investigated using a Texas Instrument Differential Scanning Calorimeter (Q-100 DSC) to better understand the transience of the LTP in the sintered alloys and the effects processing variables had on heat flow. The In Sn/In alloys were hand weighed and mixed to ensure homogeneity. Sn/In solder alloys were placed in DSC Tzero-Aluminum pans with an average mass of 25 milligrams. Excess moisture was avoided by placing samples in a vacuum desiccator for fixed intervals.

Post DSC samples were mounted in epoxy and polished or freeze-fractured to expose the microstructure of alloys. The microstructures of TLPS alloys were examined using scanning electron microscopy (SEM)

5. PREDICTED AND EXPERIMENTAL RESULTS

5.1 Expected DSC Results for Metal Alloys

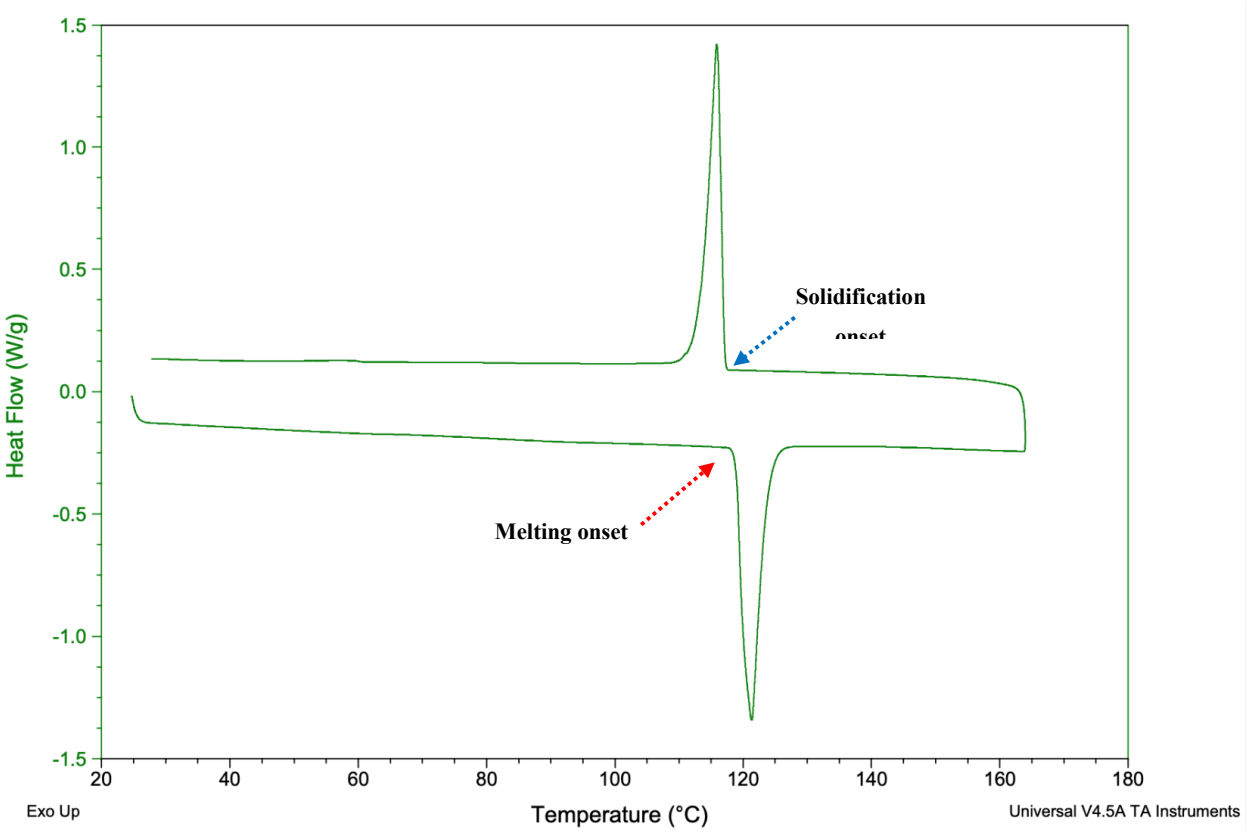

Figure 15 DSC trace for a Sn-In Eutectic alloy processed at 165°C

The typical DSC trace for a eutectic alloy is depicted above in figure 15. The negative heat flow signals of the y-axis represent the endothermic output and the positive heat flow signal of the y-axis represents the exothermic output for the solder alloys. When the alloys approach the onset of melting (marked by the red-dashed line) there is a dip in the baseline followed by a melting peak of the bulk eutectic components. Following the heating of the samples, alloys are cooled with a cooling rate of 10 °C/min. The blue-dashed line represents the onset of solidification. Generally,

for a well-mixed eutectic alloy it common for the peak area of both the endotherm and exotherm to be equivalent and the of ratio (exotherm: endotherm) to be near unity.

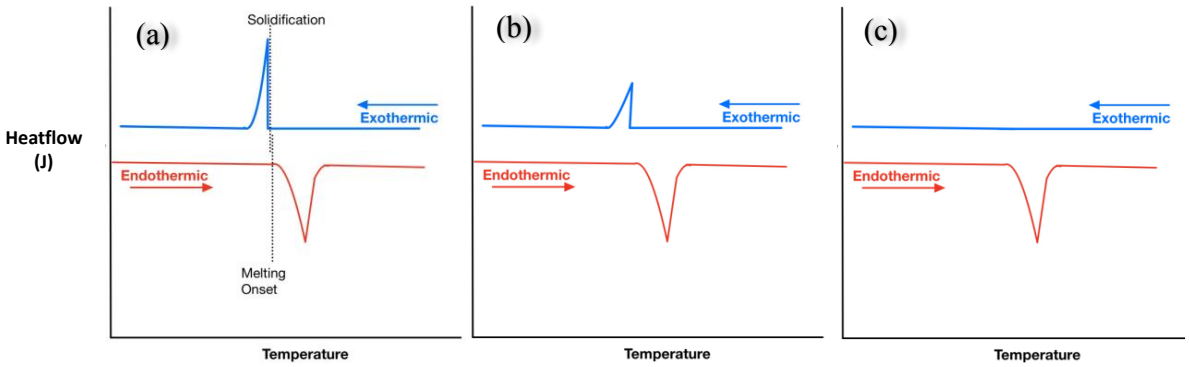

Figure 16 Schematic DSC curves forecasting evolution trends for composition and time.

In the case of alloy concentrations that are far from eutectic concentration, different trends are expected. Firstly, the case of an alloy with an overall concentration in the single-phase will be considered. Figure 16 displays the DSC signal where the top blue line indicates the exotherm and the red line indicates the endotherm. At some short times, the DSC signal will be represented by Figure 15 (a) and should have the largest exotherm area. At intermediate times the exotherm area should decrease denoting diffusion and reacting Figure 15 (b). At the end of isothermal solidification stage in TLPS, the DSC signal should be relatively flat as in figure 15 (c). A similar trend would happen if figure 15 (a) represented a two-phase region, figure 15 (b) represented the boundary of a two-phase and a one phase region, and figure 15 (c) represented a single-phase region which could react to completion. The main contrast in the second scenario is that the compositional evolution's area under the curve for the heat of fusion (endotherm) would diverge depending on the alloy's constituents.

5.2 DSC Results Components

Table 6 In-52% Sn-48% Eutectic DSC Results

SnIn-Eu	Melting Peak C	Onset Temp C	Solid1 Peak C
R3_1B1	122.98	119.3	n/a
R3_1B2	122.26	119.35	115.73
R3_2B1	122.18	119.18	115.75
R3_3B1	122.15	119.19	115.42
	Avg Melting Peak C	Avg Onset Temp C	Avg Solid Peak C
	122.4	119.3	115.6
	SD Melting Peak C	SD Onset Temp C	SD Solid Peak #1 C
	0.39	0.08	0.19

DSC analysis was run on the eutectic solder pastes (Table 6). For the indium tin eutectic solder paste purchased from Indium Corporation the onset melting temperature of 119 °C is in agreement with the Isomaki computational phase diagram. The approximate solidification peak of the tin indium eutectic powder is 115 °C.

Table 7 Sn-Foil and Sn-Paste DSC Results

Sn Foil	Melting Peak C	Onset Temp C	Solid1 Peak C
R1	237.39	233.66	188.58
R2	236.73	233.09	188.85
R3	236.71	233.06	193.44
	Avg Melting Peak C	Avg Onset Temp C	Avg Solid Peak C
	236.9	233.3	190.3
	SD Melting Peak C	SD Onset Temp C	SD Solid Peak #1 C
	0.39	0.34	2.73

Sn P506D4	Melting Peak C	Onset Temp C	Solid Peak C
R1	233.74	231.18	209.53
R2	233.43	228.3	212.57
R3	233.28	228.52	212.08
	Avg Melting Peak C	Avg Onset Temp C	Avg Solid Peak C
	233.5	229.3	211.4
	SD Melting Peak C	SD Onset Temp C	SD Solid Peak C
	0.2	1.6	1.6

Tin solder paste Sn-0.7Cu-0.5Ni (Sn P506D4) was provided by Nihon-Superior Co. Japan (Sn P506D4) was compared to Sn foil purchased from Alfa Aesar (Table 7). Tin solder paste has a slightly lower melting onset temperature compared to Sn foil because it a ternary mixture. The predicted melting temperature according to the Okamoto and Isomaki phase diagram for tin is 232 °C.

5.3 DSC Liquid Fraction Results for Alloys

DSC traces for the 10% compositional range from 74% Sn to 84% Sn were evaluated at various times and temperatures (Figure 17). Solders alloys processed at 125 ° C, 135° C, and 165 ° C did not show signs of precipitation of new phases, which is consistent with both phase diagram solvus line. For reaction temperatures of 125 °C and 135 °C the diffusion rate from time equal to zero minutes to five is fast. After 5 minutes, the diffusion rate drastically slows down.

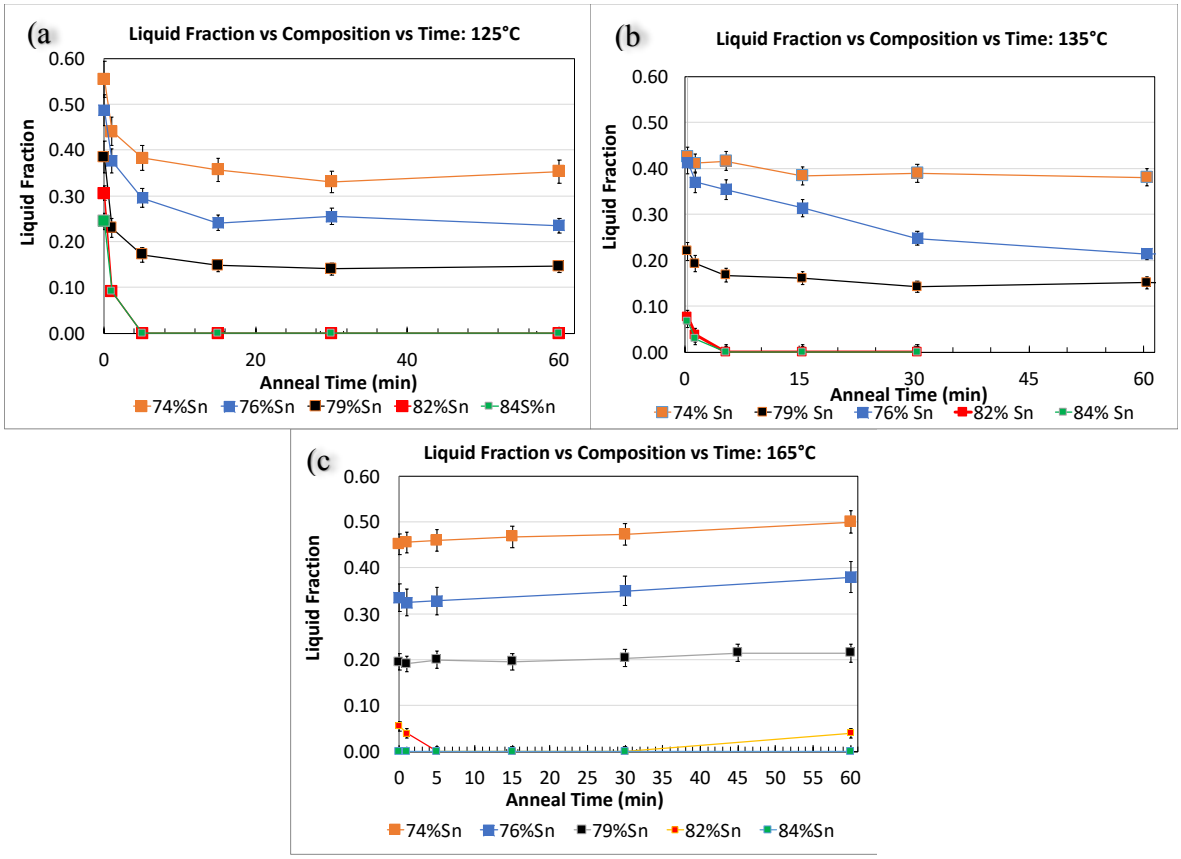

Figure 17 Liquid fraction of solder alloys measured using DSC that were processed at (a) 125° C (b) 135 ° C (c) 165 °C

At 125°C the initial liquid fraction is greatest per bulk composition, however, after 15 minutes of annealing the liquid fraction is least amongst the other processing temperatures (135°C and 165°C). According to both phase diagram 79% Sn is in the single -phase region and should completely react. The consumption of the liquid is not observed in DSC via a reduction in the exotherm. For 79% Sn alloys reacted at 165 ° C the liquid fraction plateaus. Screening of the liquid fraction values exposes a connection between the initial liquid content and temperature. The lower the processing temperature, the higher the initial expected liquid and the slower the rate of transformation. For processing temperatures of 125 ° C and 135° C diffusion slows down from 15 minutes and is hard to interpret using solely DSC. This suggests an underlying effect inhibiting further diffusion in the Sn-In solder alloys such as a reduction in the activity coefficient as the concentration gradient reduces, or oxides deterring diffusion at lower temperatures.

After melting (stage 1) and dissolution (stage 2) there is a point where the sintering densification rate reduces and temporarily alloys system maintain local equilibrium with substantial amount of liquid remaining in the system. Understanding whether it is local equilibrium predicted by the phase diagram or local equilibrium caused by kinetic factors is imperative. Only alloys of Sn-82% and Sn-84% comply to the equilibrium phase diagram projections. Figure 18 (below) delineates the effect of temperature and concentration. For alloys processed at 165°C with Indium concentrations greater than 21%, liquid remains. This behavior is representative of the 2-phase (γ+Liquid) region in the tin-indium phase diagram. After Sn-79%, the overall liquid remaining at 60 minutes reduces significantly, indicating that the liquid has reacted, or the system is in single-phase region. Currently, it is not clear if these to occurrences are mutually exclusive. Solder alloys processed at lower temperatures contain nearly three times the amount of liquid than equilibrium calculations.

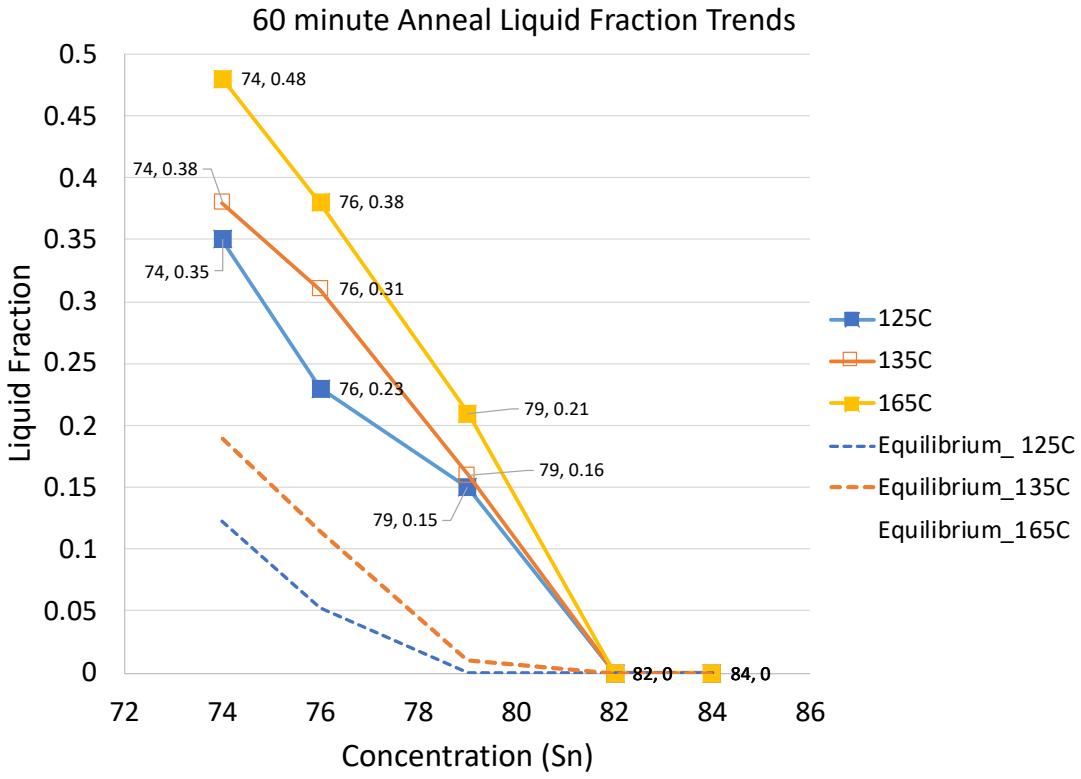

Figure 18 Liquid fraction vs concentration for alloys isothermally held for 60 minutes

5.3.1 Revisiting the Reaction Couple

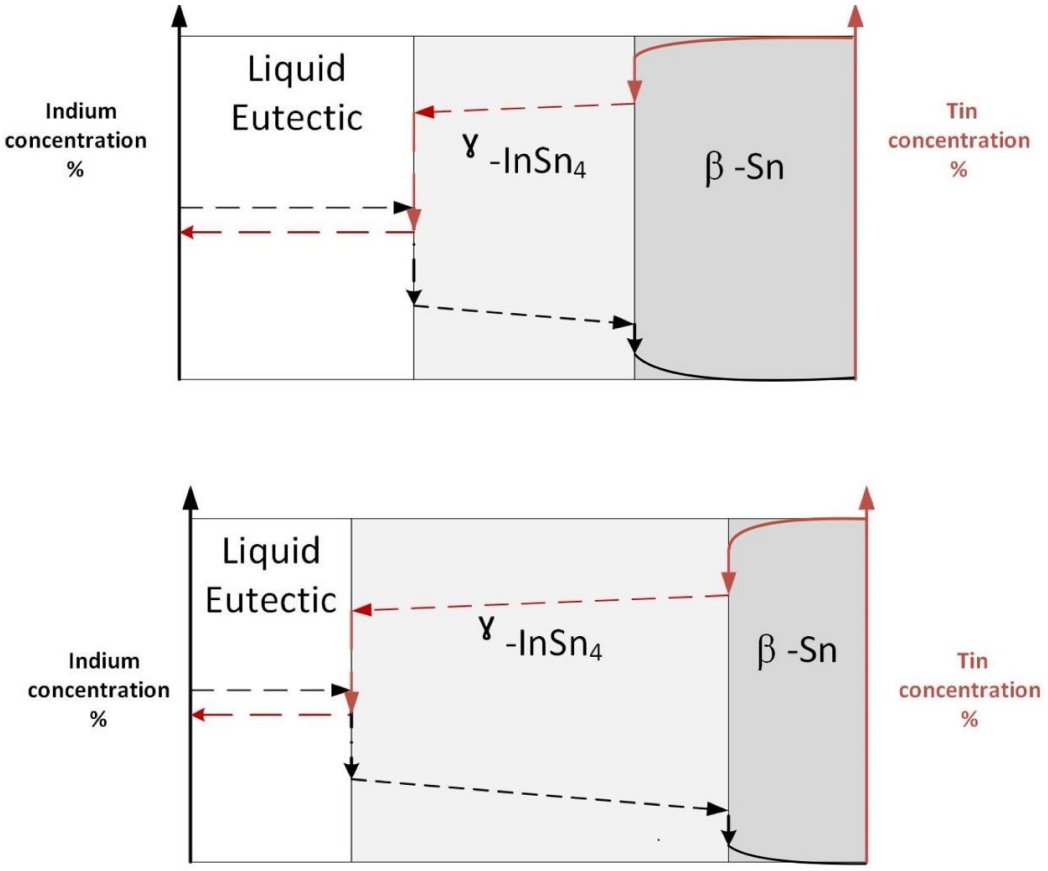

Figure 19 A modified reaction couple. The top image is the original reaction couple. The bottom image is the reaction couple that takes into consideration the reaction kinetics. Notice the increase in the γ phase. As the γ phase expands the increased diffusion length is believed to result in the slower reaction of the liquid and increased completion time for isothermal solidification (stage 3).

5.4 Confirmation of the Gamma Phase Using DSC

Only when the processing temperature is raised to 185 ° are secondary exotherm peaks observed which represent the precipitating In0.8Sn0.2 (γ) phase (Figure 20) during cooling from the liquid. DSC variance can be attributed to the mode of reaction, the relative small sample size used, and the DSC probe sensitivity.

Table 8 Liquidus line calculations compared to DSC measured values

	Okamoto	**Isomaki**	**DSC**
Concentration at%	Liquidus Boundary Temp ℃	Liquidus Boundary Temp ℃	Liquidus Boundary Temp ℃
74	184	184	181
76	188	187	183
79	194	194	-
82	200	200	-
84	204	203	-

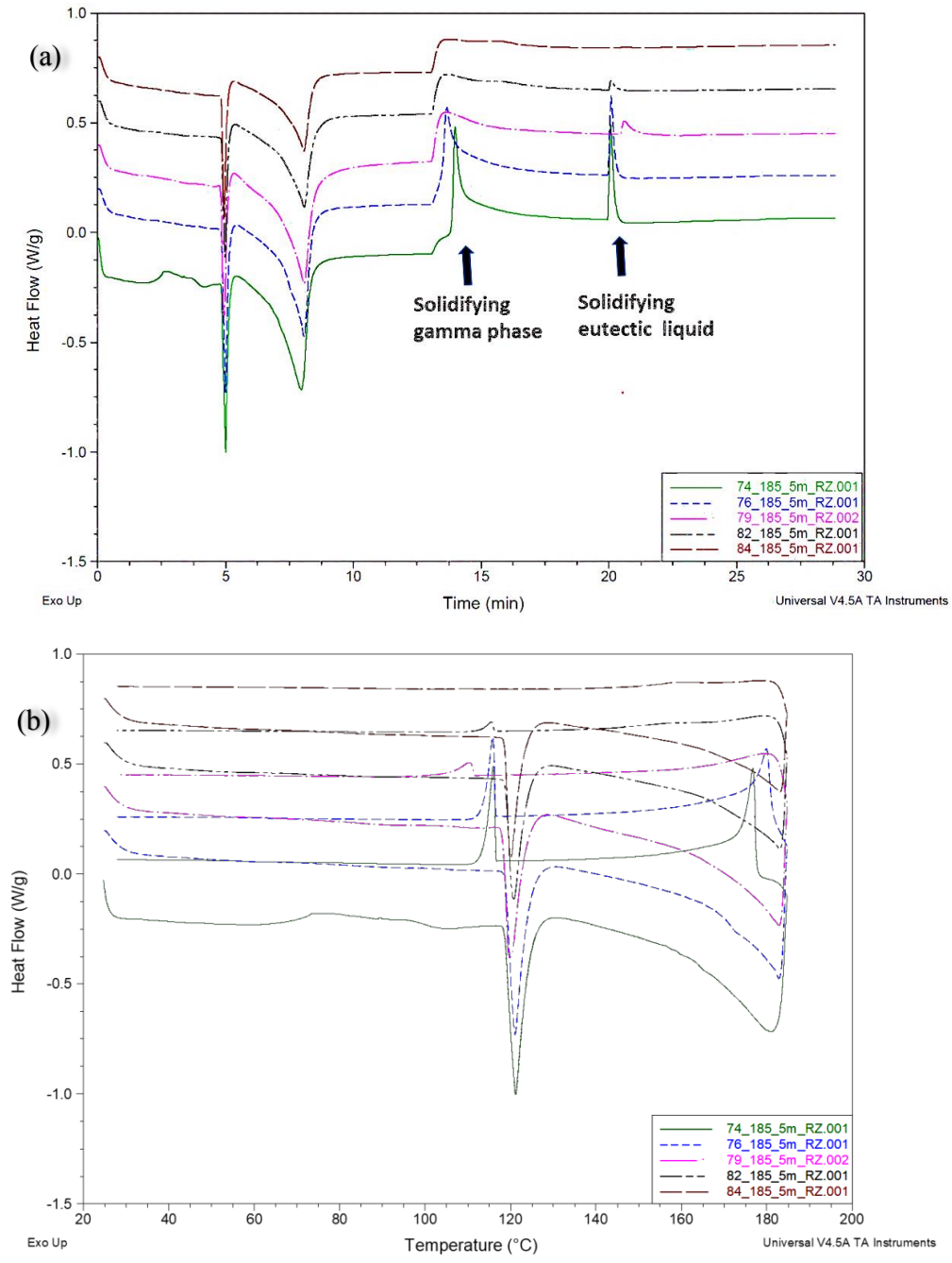

Figure 20 DSC curves for concentration (74 to 84) processed at 185 ° C with a 5 minute isothermal hold. (a) Time vs Heatflow DSC curves (b) Temperature vs Heatflow DSC curves

5.5 DSC Results Cycled Experiments

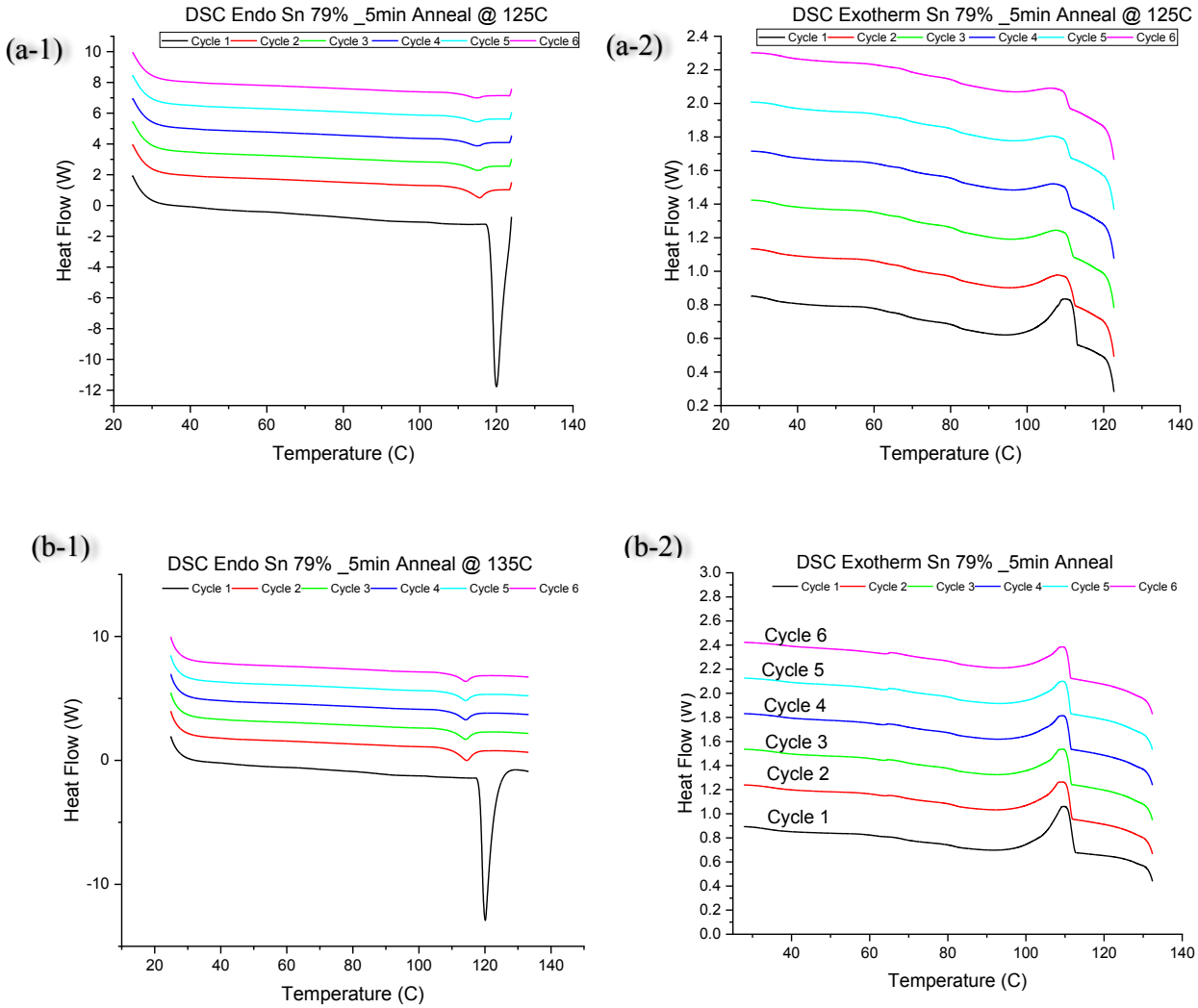

Figure 21 DSC Data for Sn-79% solder alloys annealed 5 minutes per cycle (a) 125 C cycled six times (b) 135 C cycle six times

Samples were cycled to understand thermal and diffusional effects of processing (Figure 21). The multiples cycles reveal after the initial five-minute treatment (at 125°C), 135°C), and 165°C) very little change in the endotherm or exotherm occurs - inferring the liquid remaining is reacting very slowly.

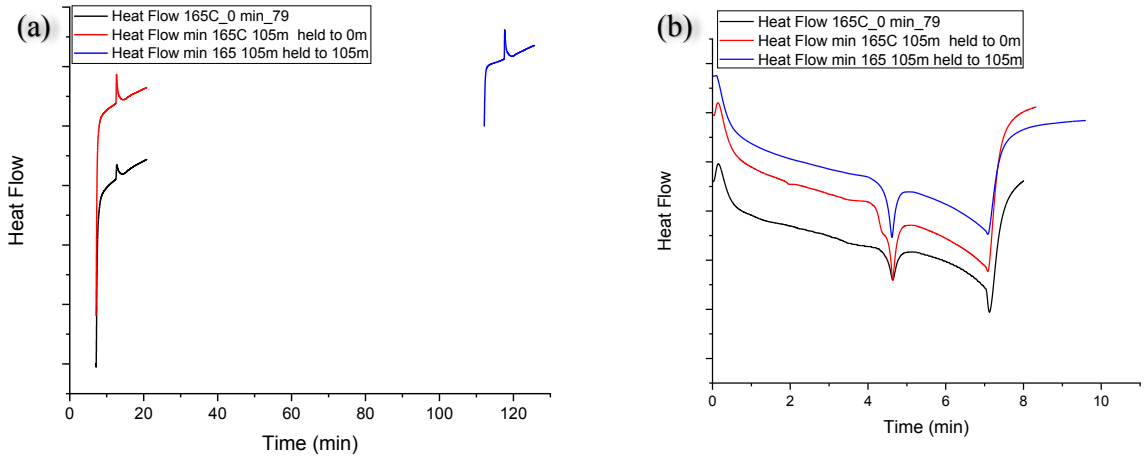

Figure 22 DSC Plots for Sn-79% alloys that have been cycled twice (a) exotherm (b) endotherm

Alloys that were cycled at temperatures 165 °C (46° C above the eutectic temperature) result in an almost immediate plateau as seen Figure 17 (c). Three different alloys of Sn-79% have been cycled twice in Figure 22. (1) The DSC traces in black trace represent an alloy that was annealed without hold, and then repeated. (2) The red represents an alloy annealed for 105 minutes, and then cycled without an anneal time (0 min). (3) The blue curve represents an alloy that was annealed for 105 minutes on the first cycle, and then annealed to 105 minutes again on the second cycle. For all samples annealed, the second cycle exotherm: endotherm ratio is nearly unity. Apart from some artifacts that may stem from the DSC probe sensitivity diffusion seems very slow.

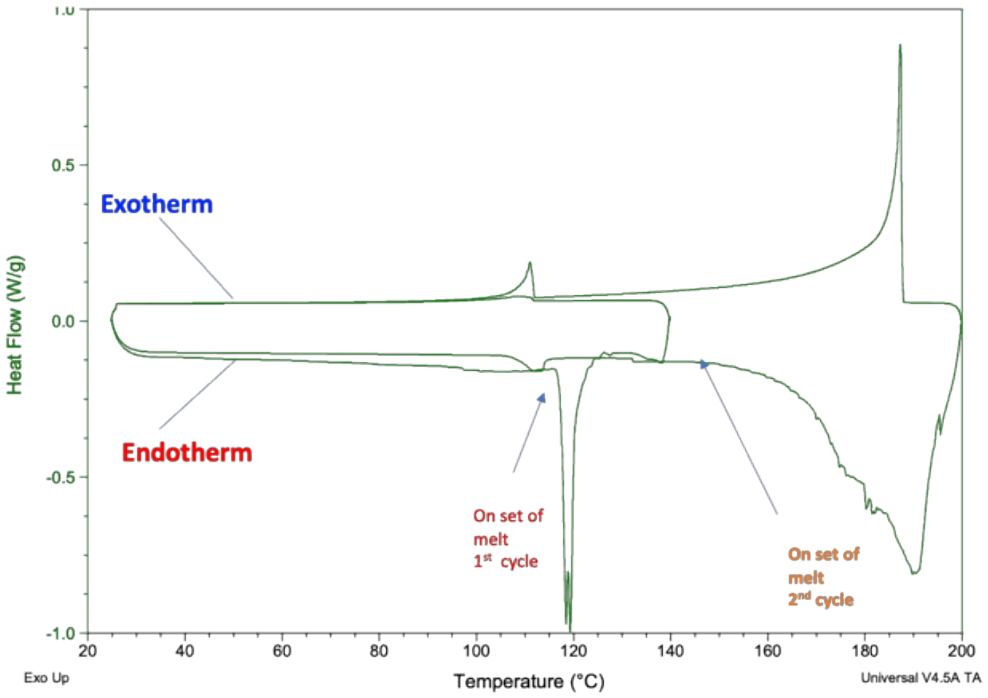

Figure 23 DSC Plots for Sn-79% First anneal at 130° C with an isothermal hold of 10 minutes, and cooled. After cooling the sample was heated to 200 °C

Originally in Figure 23 the Sn-79% alloys, was processed at 130 °C and a large endotherm peak at an approximate onset of 119 °C is apparent. When the alloys are cooled on the first cycle a very small exotherm peak is observed at approximately 112°C. On the second cycle the sample alloys is heated to 200 °C. The second cycle's endothermic peak is much smaller in comparison to the first cycle, indicating most of the eutectic liquid has reacted. Furthermore, during the cooling cycle, a sharp exotherm peak is apparent at approximately 187 °C indicating the solidification of the In0.8Sn0.2(γ) phase and a secondary solidification of the remaining eutectic liquid peak at 112 °C. A mirrored effect can be seen in the area of exotherm and endotherm, for cycle one and cycle two. The area of the endotherm associated with the eutectic liquid reduces after cycling, while the area of exotherm associated with the eutectic liquid area increases as temperature is increased. This increase in the eutectic liquid upon cycling is counter intuitive.

6. MICROSTRUCTURAL EVOLUTION

The following schematic in Figure 24 is the predicted equilibrium microstructure of the Sn-In system. Based on the equilibrium phase diagram bulk composition and anneal time, IMC growth and lamellar structure were expected to be observed. Theoretically the differing alloy's bulk compositions and anneal time should have a significant impact on the phase transformation as well as the reaction path manifesting in distinct microstructures. The predicted microstructure assumes very slow cooling from the liquid.

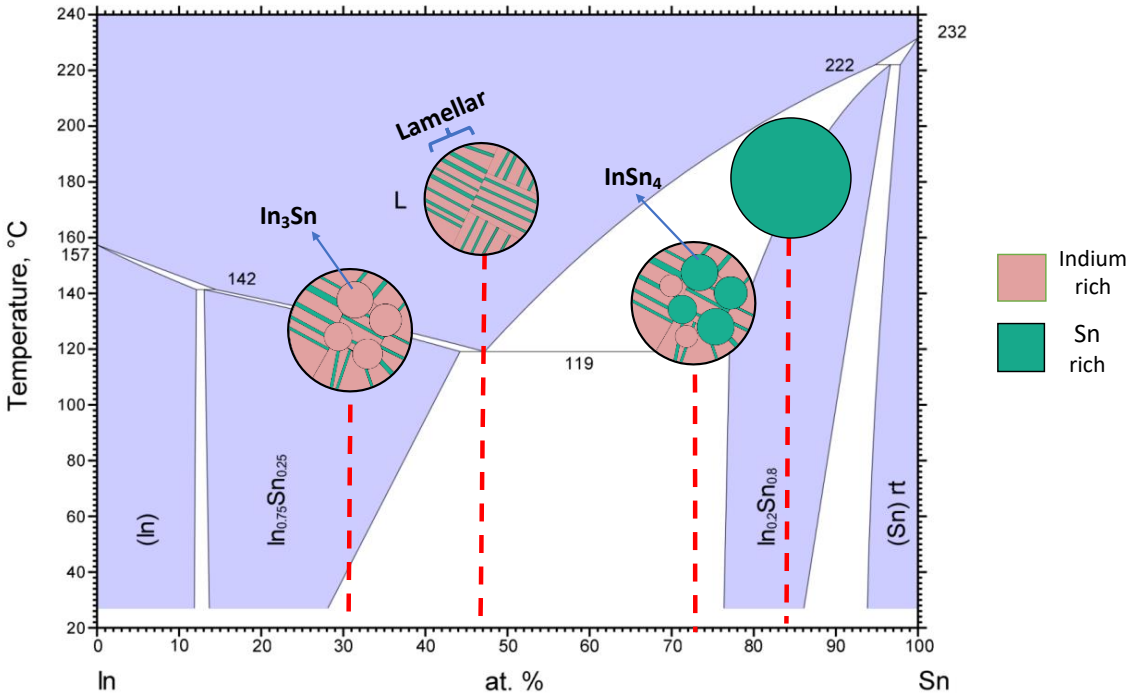

Figure 24 Theoretical equilibrium microstructure predictions using the Isomaki phase diagram. The red lines only indicate position.[17] [25]

6.1 Predicted Microstructure Based on TLPS

The predicted microstructure (Figure 25 below) interprets TLPS for two different scenarios. Case 1 when TLPS goes to completion with the majority yield of the γ-intermediate phase and case 2 a metastable case when gamma yield is low owing to an interruption of the reaction (prior to completing isothermal solidification) or when the reaction is limited by kinetics factors. For Case 1 the system is heated sufficiently, and the dissolution of Sn occurs, followed by diffusion and isothermal solidification. At the end of case 1 the alloys will transform to mainly γ- $InSn_4$. For Case 2 if the process is stopped prior to completion of the isothermal solidification the resulting microstructure may have eutectic liquid, β-Sn, γ- $InSn_4$, and In_3Sn. In both cases there can be isolated areas due to limited contact since the samples are not mixed while reacting. Lack of mixing may contribute to slow diffusion reaction depending on one's path and parameters, especially for low processing-temperatures.

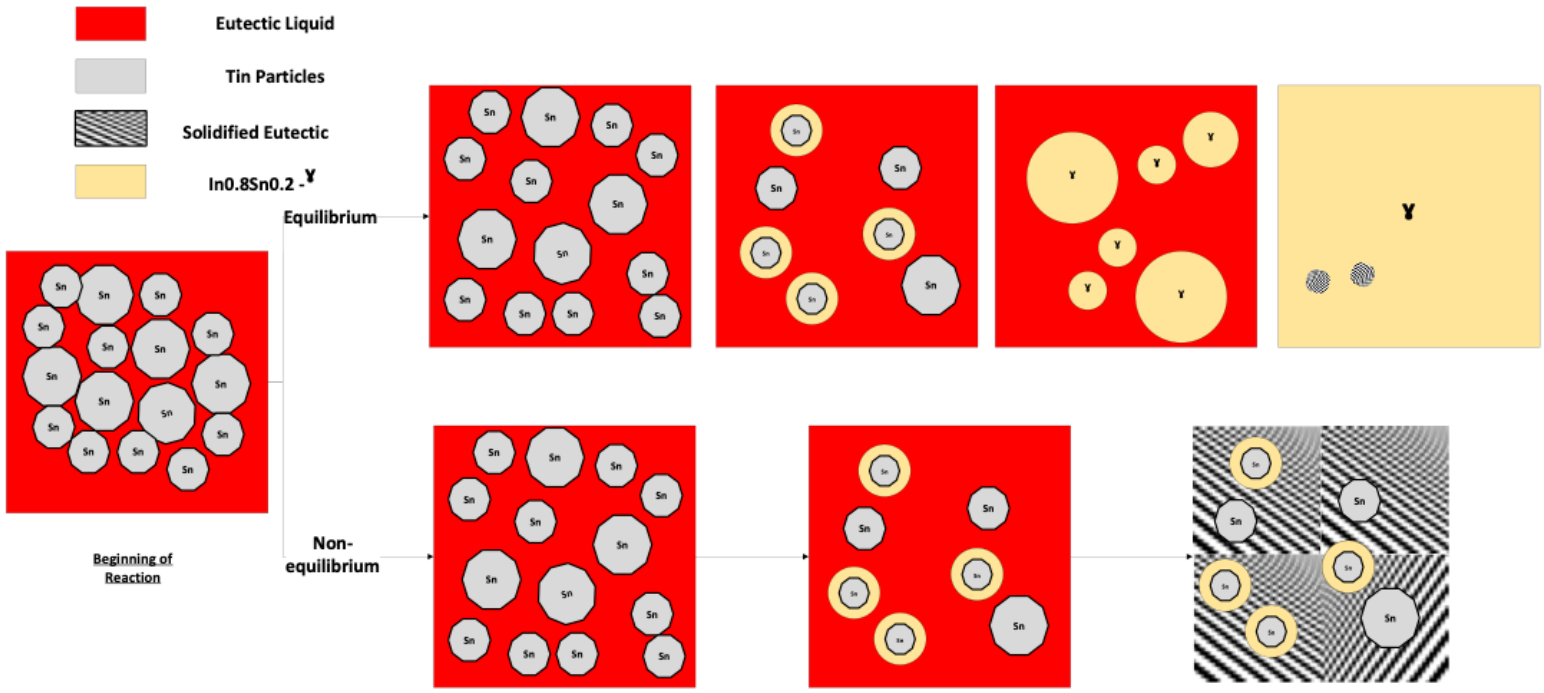

Figure 25 TLPS Schematic for two instances. (1) Complete reaction with a majority yield of the γ-intermediate phase. (2) Limited transformation yield of γ-intermediate due to interruption of the reaction the reaction or kinetic facto

6.2 Microstructural Evolution After Short Periods

Sample preparation of Sn-In alloys was very challenging due to Indiums softness as reported by Sandia National Laboratory [26]. However, freeze-fracturing of solder did expose the visible surface for microstructural analysis. The combination of DSC and microstructure analysis provides information on the reaction kinetics. Improvements to sample preparation will enable higher accuracy to the compositional analysis obtained with EDS, and the crystallographic information obtained from EBSD.

It is challenging to differentiate between $InSn_4$ - γ tin rich regions and β-Sn regions, or In_3Sn-phase and pure Indium during topographical and compositional inspection. Previously Kubiak et al. expressed the difficulty with x-rays and recommend the use of neutron scattering to differentiate between to neighboring periodic elements [27]. Consider the microstructural evolution of tin indium for 76% and 74% tin which will aid the development of a diffusion model of the eutectic liquid into tin. Note that the porosity reduces in the system over time for the two different compositions.

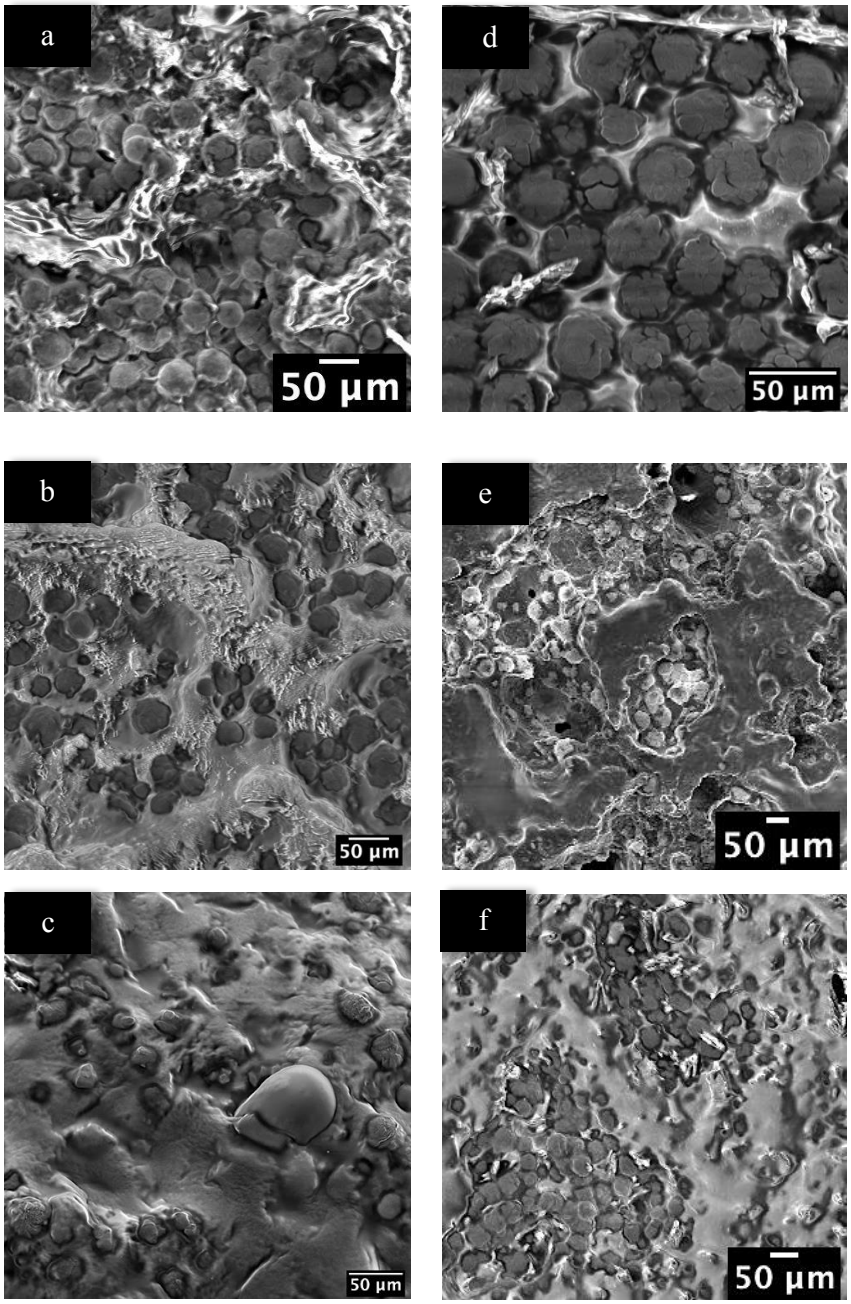

Figure 26 Sample processed at 125 °C Secondary Electron Micrograph of the surface of alloys isothermally held from 0 to 5 minutes. Sn-76% for times (a) 0 minutes, (b) 1 minute, (c) and 5 minutes. Secondary Electron Micrograph for Sn-79% for times (d) 0 minutes, (e) 1 minute, (f) and 5 minutes.

Both concentrations of tin (76% & 79%) were annealed at 125°C for multiple times as depicted in Figure 26. During annealing the LTP liquid wets the tin particles and continues to do so as it reduces the voids seen from 0 minutes to 5 minutes. Observing the microstructure of the solder paste is challenging, so the surface of the solder was observed during short times. At 125° C, no precipitating phases are observed nor is the eutectic lamellar structure visible. More wetting and distortion of spherical particle can be noted (comparing the initial 0-minute microstructure to that of 5-minutes).

6.3 Microstructure After Longer Times at 165°C

The following samples have been annealed for 60 minutes at 165°C using DSC. The microstructure of the selected compositions is freeze-fractured. All samples seem to display signs of segregation with some void formations. Currently it's unknown if cryo-cleaving contributes to the voids. The darker regions in the following sample are indium rich regions, while the lighter region are tin rich regions as noted by J. Morris et al. [28]. Topography of the solder can be observed using secondary electrons, and qualitative compositional analysis is done using a backscatter detector.

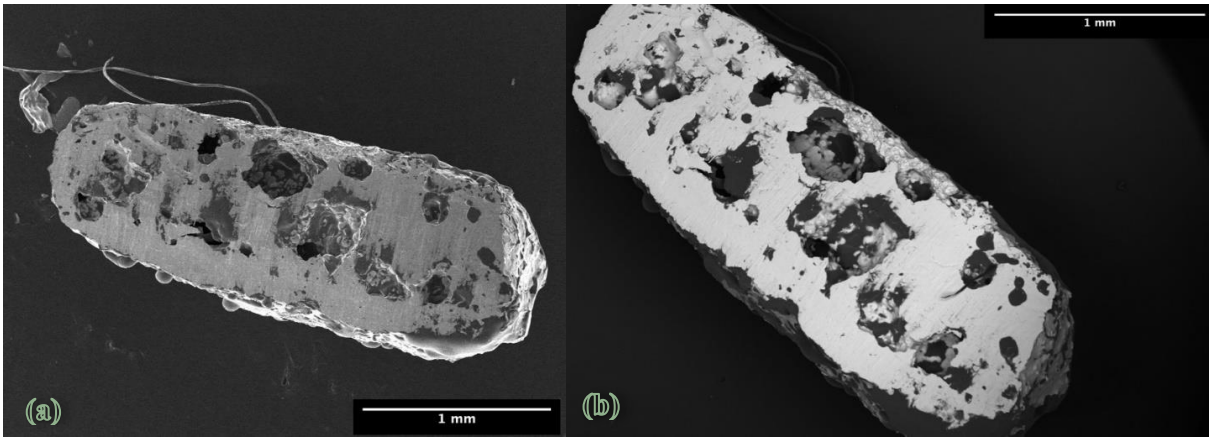

Figure 27 Fractured solder sample containing tin-indium Sn-74% annealed at 135°C for 60 minutes (a) Secondary image (b) backscattered image of the sample

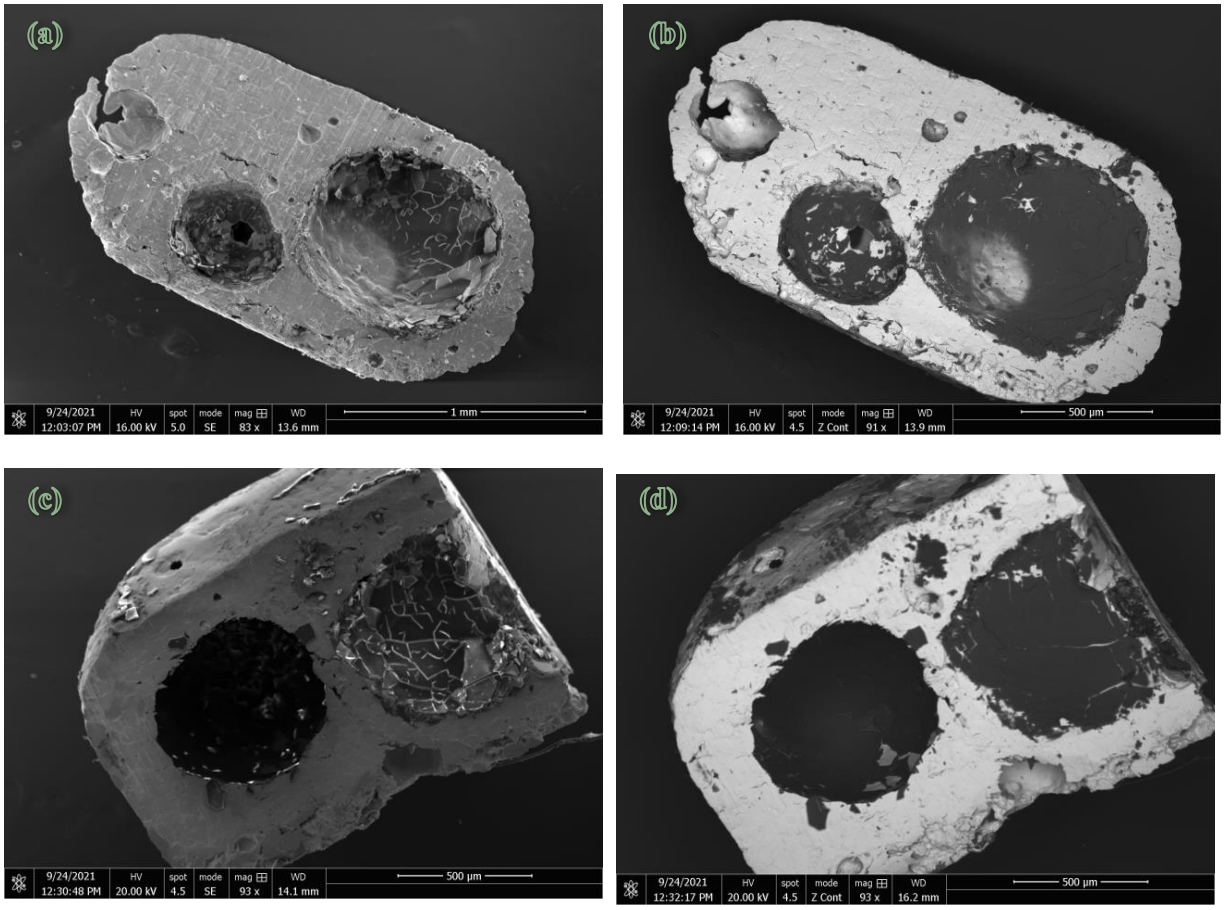

Figure 28 Fractured solder sample containing tin-indium Sn-74% annealed at 165°C for 60 minutes (a) Piece 1 hemisphere secondary image (b) Piece 1 hemisphere backscattered image of the sample (c) Piece 2 hemisphere secondary image (d) Piece 2 hemisphere backscattered image of the sample

Holding all parameters constant but increasing the reaction temperature by 30 degrees impacted the microstructure of the solder. Alloys processed at Sn-74% contain less porosity, however they have large cavities. There seems to be regions that undergo self-segregation. Figure 27 (a and b) represents one half a sintered solder alloy, and Fig 27 (c and d) represents the other side of the same sample. Backscattering for compositional identification reveals that the darker region in figure 28 (b) and (d) are indium rich regions. By inference of the topography, some indium rich regions apparently undergo brittle fraction.

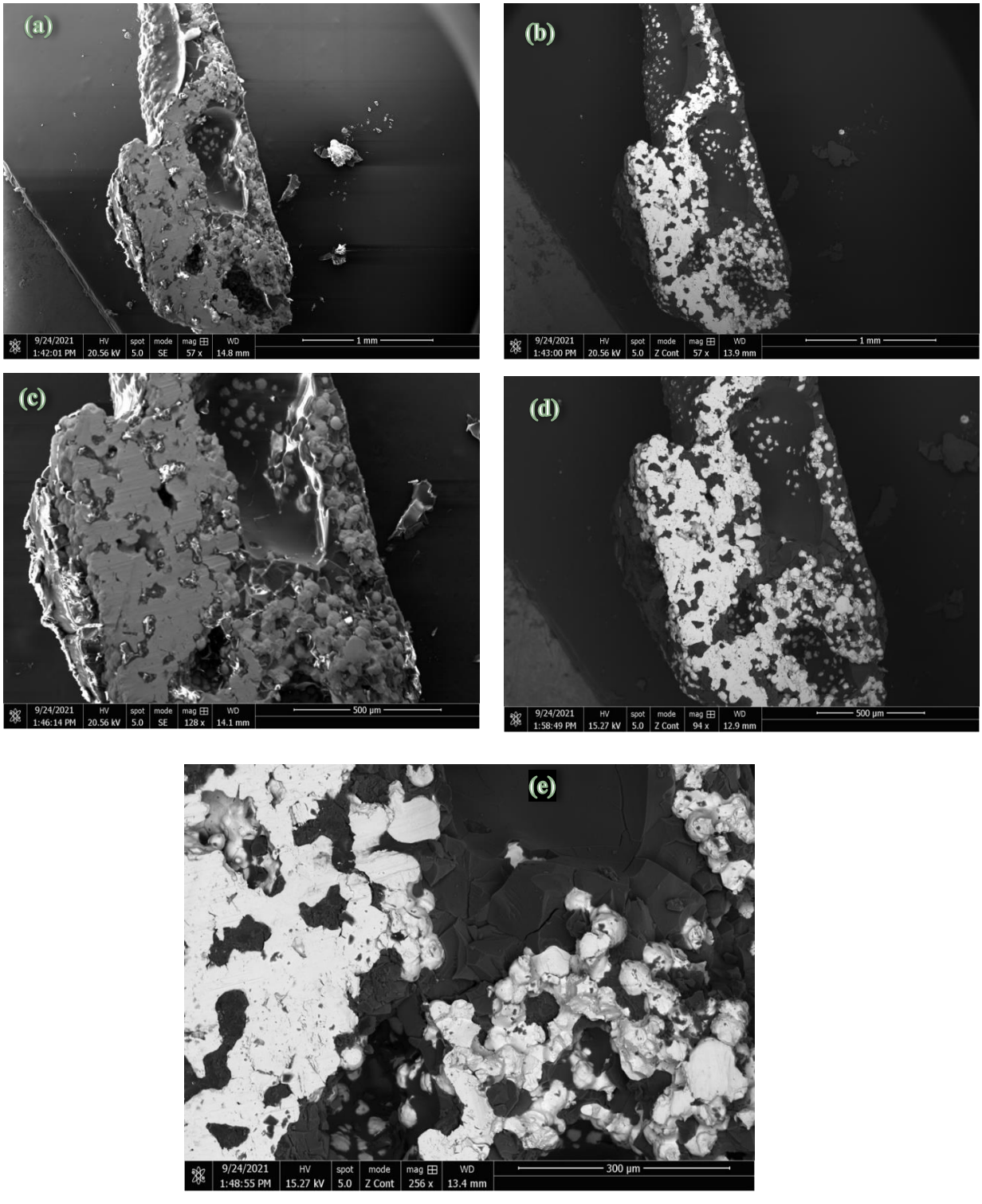

Figure 29 Fractured solder sample containing tin-indium Sn-84% sample annealed at 165°C for 30 minutes

The microstructure of solder alloys with the lowest indium content is displayed in figure 29 above. According to DSC, the liquid within the alloy is completely consumed after annealing for 1 minute. Although the DSC reveals key information about the liquid consumption, it apparently does not provide information related to the homogeneity of the alloys.

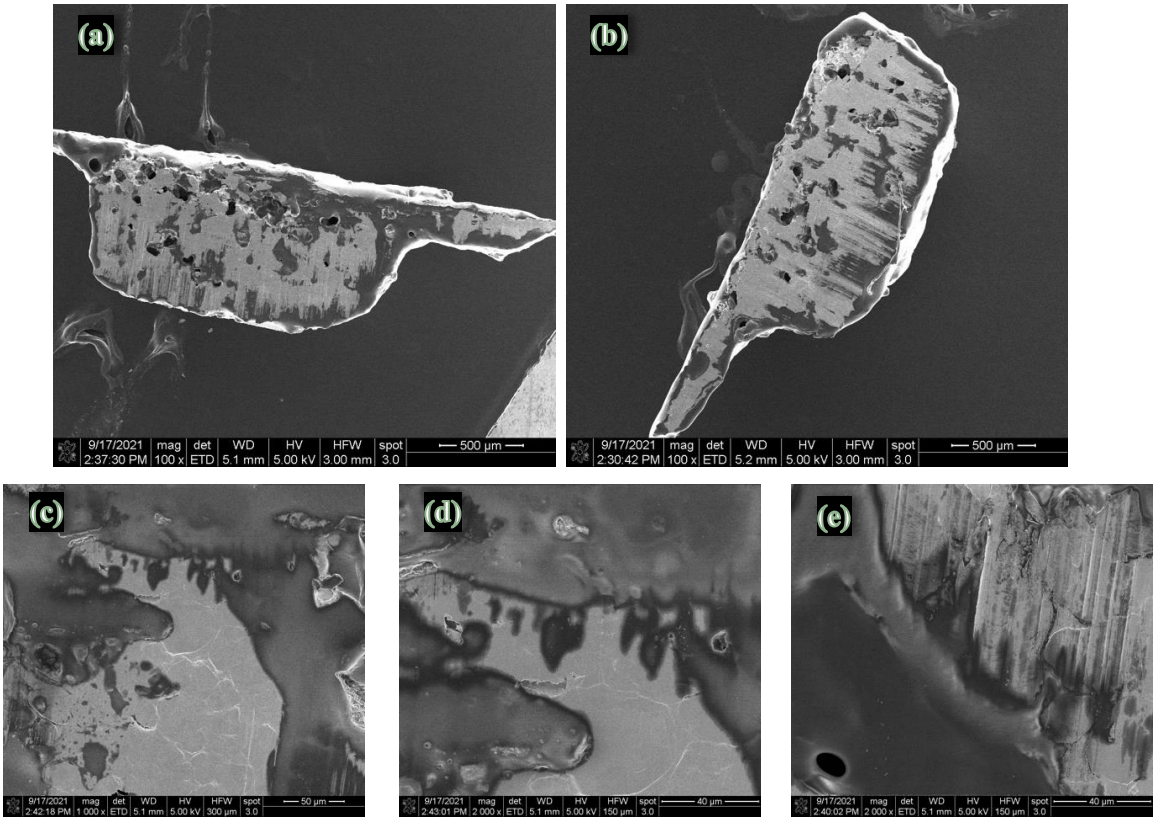

Figure 30 Fractured solder sample containing tin-indium Sn-74% annealed at 125°C for 15 minutes

6.4 Microstructure Processed at 125°C After 15 Minutes of Annealing

DSC result for solder processed at 125 °C diffusion rates showed signs of slowing down from 5 minutes and plateauing from 15 minutes onwards. Extrema compositions of Sn-74% (figure 30) and Sn-82% (figure 31) were selected for comparison. Figure 30 show two-halves of a Sn-74% cleaved solder, while figure 31 displays two different sections of one side of a cleaved solder

sample of Sn-82% composition. Overall, Sn-74% alloys with more indium content seem to have less continuous pores, appear smoother, and contain less void fraction. Although a higher indium composition may increase wetting, pores size is also related to the cooling rate used for the solder alloys.

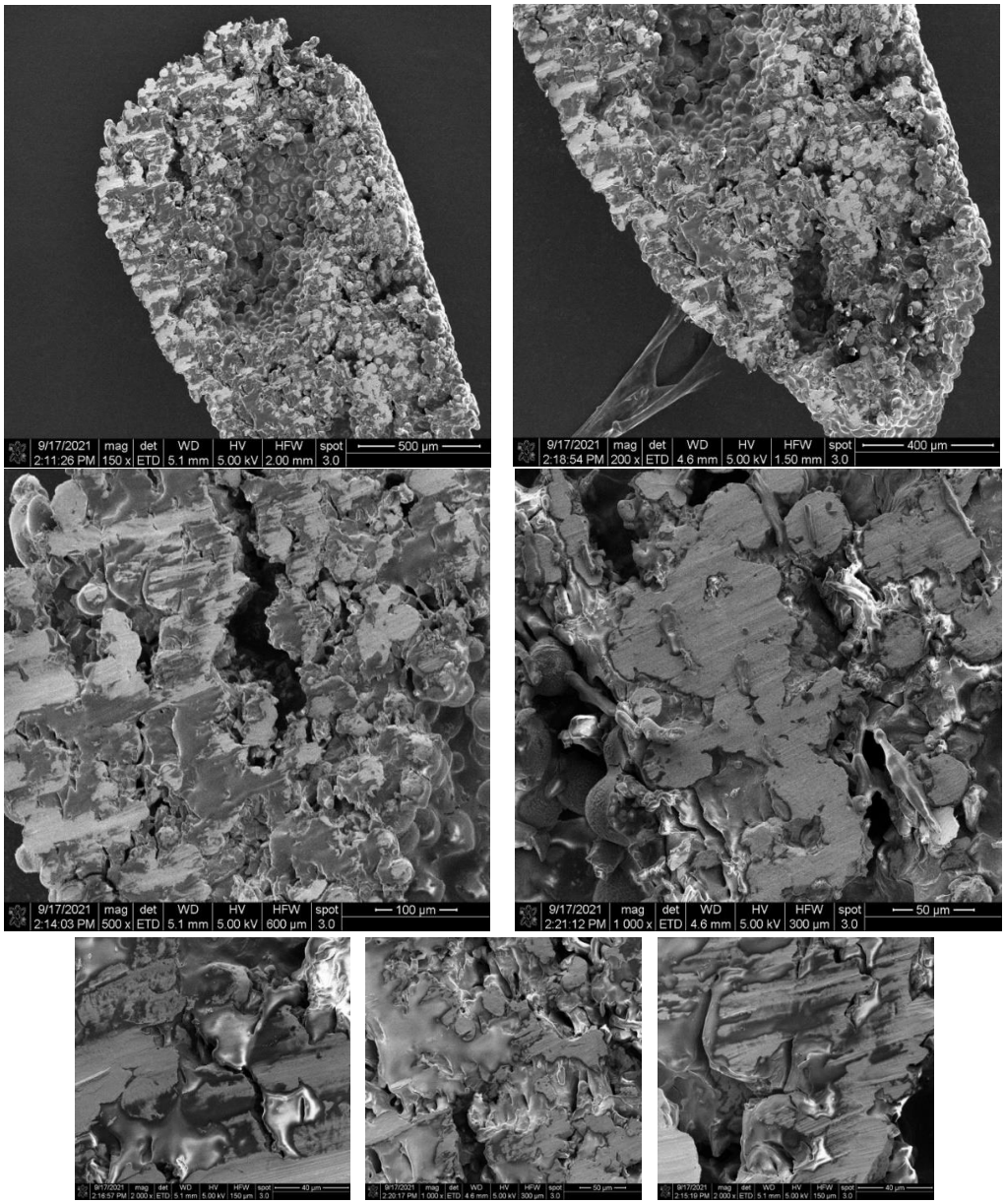

Figure 31 Fractured solder sample containing tin-indium Sn-82% annealed at 125°C for 15 minutes

6.5 Processed Eutectic Microstructure

The lamellar structure is not observed for the processed Sn-In eutectic solders. Further processing such as chemical etching or ion-polishing with non-gallium sources may expose the lamellar structure. Similar regions of segregation are observed in the alloys and are also noted in the eutectic alloys. The mode of the reacting reactants has a larger significance when the constituents are not in the same phase (solid, liquid, gas etc.). In example, a eutectic mixture that is powder in nature, and a eutectic mixture that has been liquified prior at lower temperature, may result in differing microstructures.

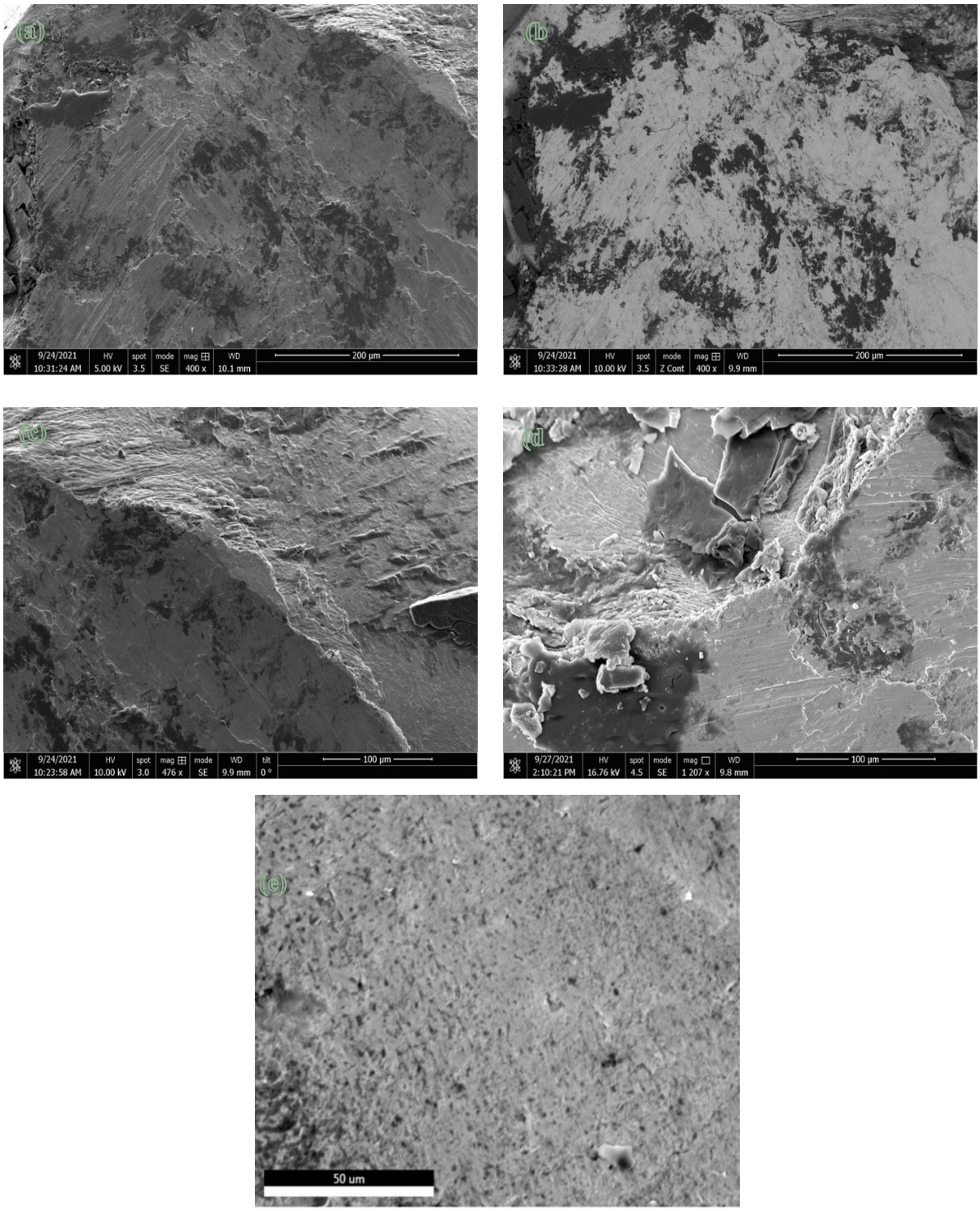

Figure 32 Tin-Indium eutectic solder paste processed at 180° C without any isothermal hold that has been freeze-fractured to reveal the microstructure. Multiple sides were cleaved and analyzed

6.6 Electron Dispersive Spectroscopy (EDS) Results

Freeze-fracturing creates surfaces of different heights and roughness. This difference in height may impact the interaction volume and therefore impact the quantification capability of EDS to some extent. Regardless, EDS analysis of solder alloys was conducted. Overall values for the following sample are not far from the overall formulated composition. For most EDS mapped sample there is a slight under-estimation of the Sn % (Table 9).

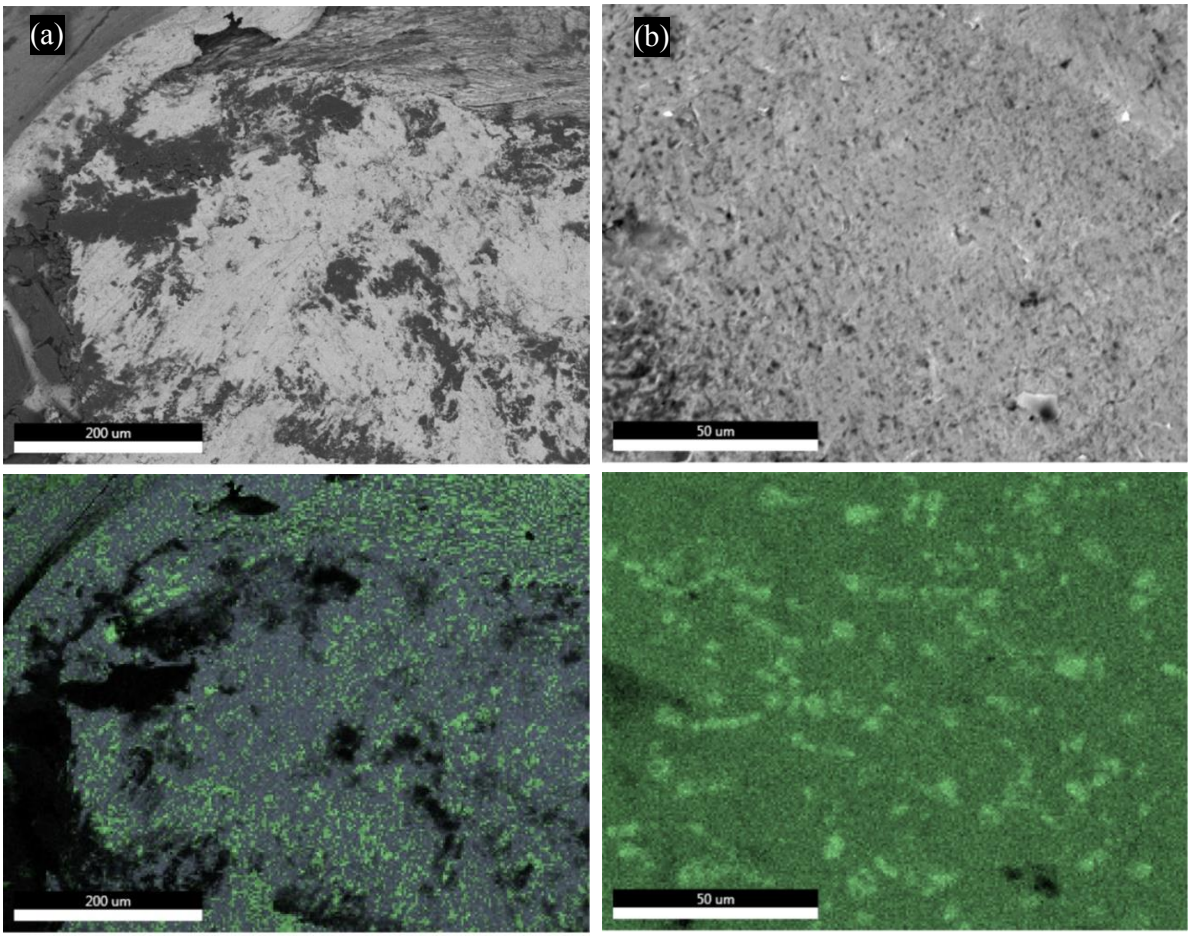

Element	Wt%	At %	Error %
In	50.58	51.41	2.14
Sn	49.42	48.59	2.18

Element	Wt%	At %	Error %
In	48.45	49.28	1.74
Sn	51.55	50.72	1.68

Figure 33 Eutectic Tin-Indium EDS results of different regions

Table 9 EDS Results for samples with Sn concentrations of Sn-74% and Sn-84%

Sample Composition		EDS Map of Comp. of Sn	Temperature °C	Time
Sn	In	Tin Rich Phase		**min**
74	26	73.5	135	60
74	26	72	165	60
84	16	81.9	165	30
Values are indexed in atomic %				

7. MODELLING TLPS INTERACTIONS

7.1 Simple Microstructure Model

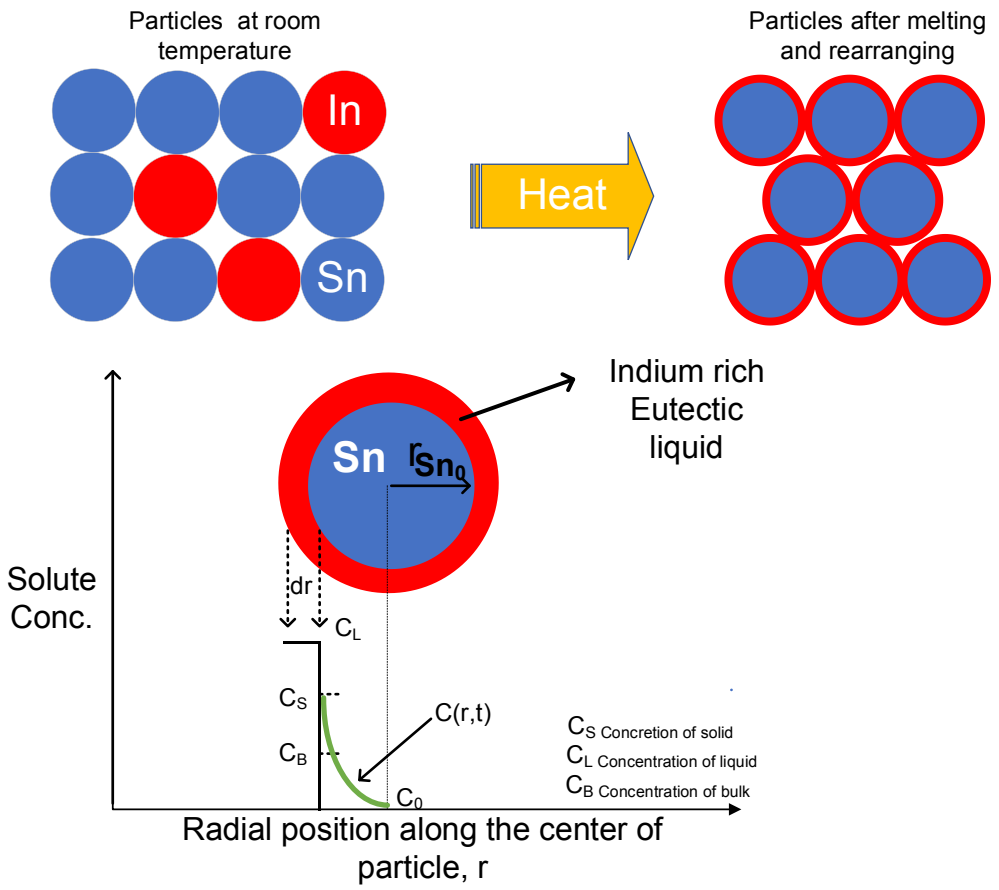

Figure 34 Simple Model for TLPS focusing on the isothermal thermal solidification stage (3) [15]

It is assumed dissolution is rapid and t=0 marks the beginning of the isothermal solidification stage. At t=0 C_L is the original solute concentration of Indium is the same as the liquidus boundary line and C_o is the original tin (HTP - Sn). C_s on the other hand is more challenging to approximate because IMC growth may be competing with other expected solid phases ($InSn_4$, $InSn_4$+ β-Sn). In many cases the reaction has been considered mainly using 1-D net motion approximations. With such approximations, deviation is challenging to account for. A simple model of the

microstructures predicts that the Sn particles are coated by a liquid interphase. Figure 34 depicts the starting liquid in red as *dr*. During TLPS the eutectic liquid and solute within the eutectic liquid is decreasing due to conservation of mass. Simple kinetics predicts for large Sn particles diffusion of solute into the center will take longer. This is one rationale for the substantial liquid found in the solder alloy post-annealing, except for higher temperatures at 165 °C. One theory is as β-Sn reacts with the eutectic-liquid a layer of gamma forms. The growing gamma phase's (Figure 35) increased diffusion length and higher density impact the diffusion rate especially at temperature near the eutectic temperature (119°C). TLPS has more contact area in comparison to a typical brazing couple reaction interface, however for solder-pastes predicted to be in a one phase region liquid remains. Over short time periods (up to 5 minutes) the gamma layer thickens and inhibits further diffusion into the Sn particle at temperatures up to 165°C for Type 3 (35 µm average) Sn-In solder. The gradient in concentration noted in the solder alloys may influence the performance of the soldered joints. Morris et al. report that the intermediate phase behaves more like a solid solution. That being, the intermediate phases' semblance to the solid solutions in their mechanical prosperities, broad solubility, and disorder at ordinary temperatures[24].

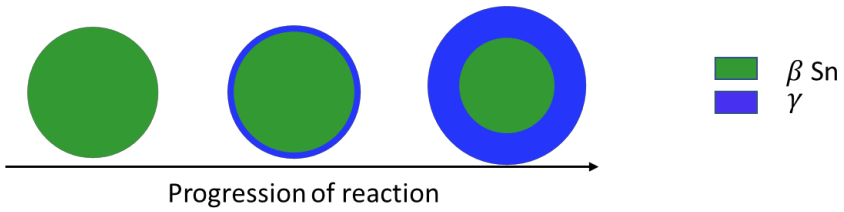

Figure 35 A schematic of the Growing InSn4- γ. The increase in the γ phase is hypothesized to affect the diffusion at temperatures lower than the liquidus boundary of that specific composition.

8. CONCLUSION AND RECOMMENDATION

A part of the motivation for this project was not achieved with the current reaction parameters. This work set out to lower the reaction temperature as low as 130° C and after the first reaction-pass an increase in the temperature tolerance to ranges greater than 200°C. Although the formation of solder joints was possible at temperature as low as 125° C, it came at the expense of the quality and an increased reaction time. Although the quality criterion was not extensively reported, the obvious voids, excess liquid, and segregation noted in the microstructure are causes of concern. Even still, for concentrations higher than Sn-79% isothermal solidification seems to have neared completion of the isothermal solidification stage.

8.1 Reaction Fabrication Using Smaller Particles

Many processing variables can impact the speed and yield of reactions. Future studies conducted on tin-indium solder should focus on reducing the particle size. Reducing the particle size allows for more reaction sites as well as increased curvature. The increased reaction sites, and increased chemical potential gradient may be able to overcome the kinetic barrier that various solder alloys experience in this study. Reduction of the particle size can be done by using Type 5 Solder paste (15 μm). An alternative means followed by Shu et. al. involves the milling of the reacting constituents and the addition of flux to facilitate the reaction by removing interference of oxides [29]. Since indium is soft in nature, it may be more useful to cryo-mill to limit particle shape deformation. Prior to reacting alloys, it is important to ensure they are thoroughly mixed. This may be achieved by mechanical mixing of paste or acoustic mixing for powdered samples.

8.2 Metallographic Examination

Sample preparation on Sn-In samples was challenging. Although freeze-fracturing was useful it also limited the accuracy for quantitative analysis. Freer et al. recommend the following recipe for obtaining micrographs. Firstly, the sample are bound in epoxy and then ground with 600 grit silicon carbide. Next 6 μm diamond paste was used, and after 1 μm aluminum powder was used. Lastly a colloidal diamond suspension polished was administered to the sample [30].

APPENDIX A.

Umantsev et al. defined the process of intermediate phase growth as simultaneous crystallization plus ordering of a growing phase[31]. In his work Umantsev, defined a free energy term as a function of crystallinity, ordering, and concentration. Furthermore, in considering the phase transformation they to different scenarios base on the processing temperature

- **Case 1: Solid-state soldering with unlimited amount of solder**
- **Case 2: Liquid-state soldering with unlimited amount of solder**
- **Case 3: Limited amount of molten solder**

From the work of Umantsev, it can be inferred that crystal structure play a role in the phase transformation. To obtain the In0.2Sn0.8 (γ-$InSn_4$), the system transforms from a tetragonal space group to a hexagonal space group (Table 3). During low temperature TLPS the reacting solder is generally never a complete liquid, since the solder system is never a liquid it may be that 1-D models of growth and diffusion overestimate the surface sites of the reacting solid/liquid interface as seen in section 3.3 Figure A.1. If the surface sites are more limited than hypothesized, symptoms of poor reaction -sites can be increased heterogeneity and slow diffusion.

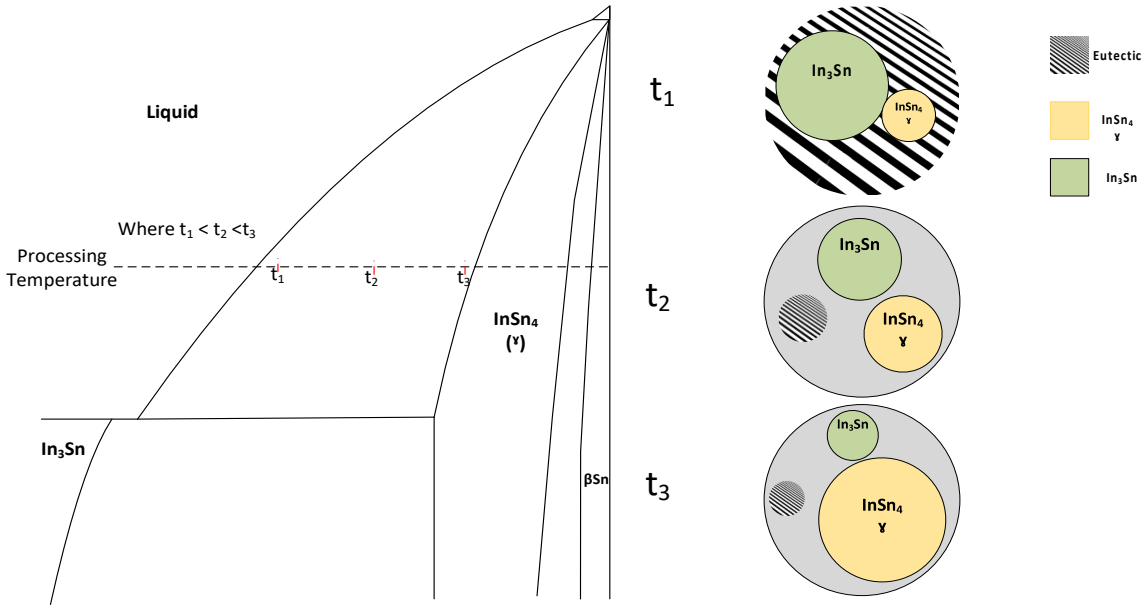

Figure A.1 Theoretical volume fraction of phases depending on the time allowed for the reaction during the isothermal solidification stage.

APPENDIX B. PLOT FITTING

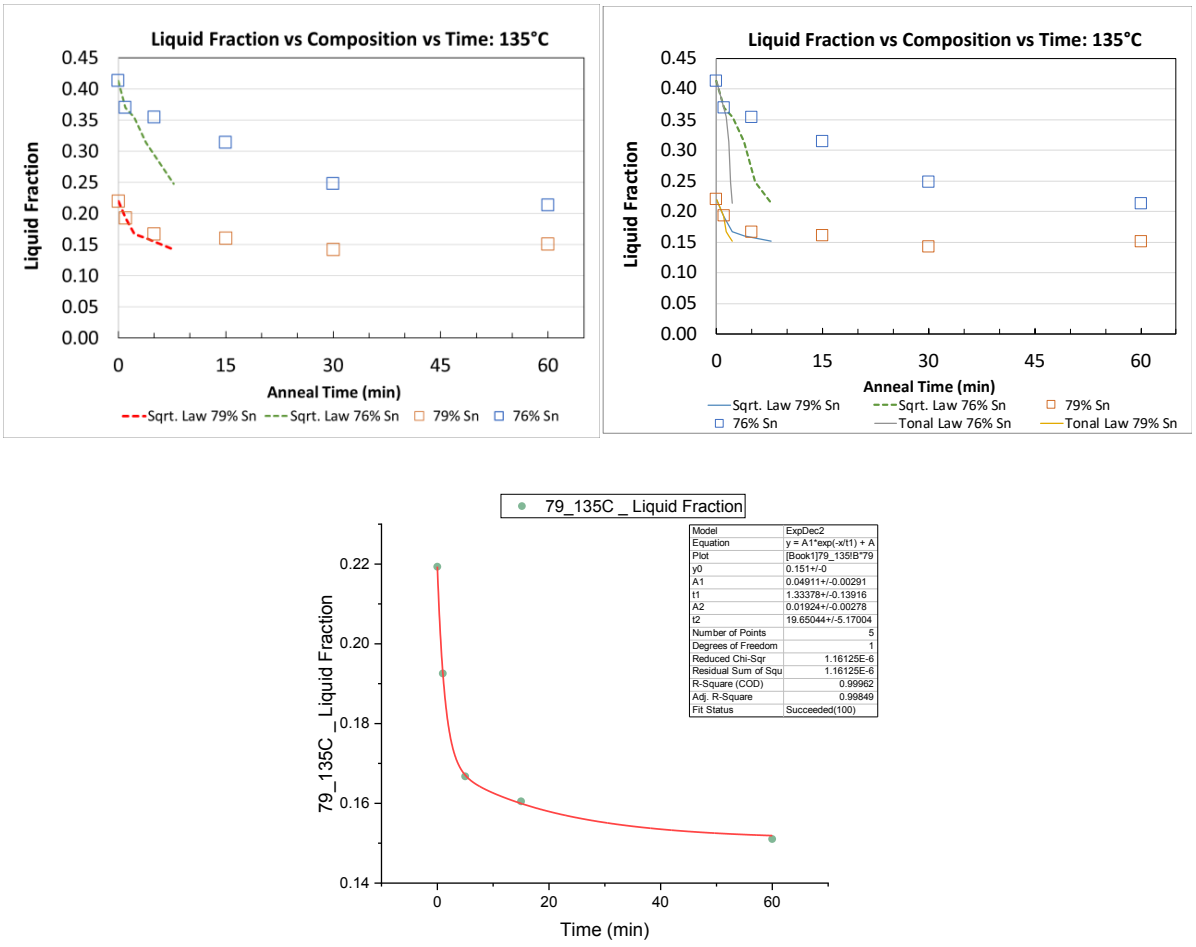

Figure B.1 Different Model fitting approaches that may be used to approximate the completion time for given composition.

REFERENCES

[1] W. Zhang and W. Ruythooren, "Study of the Au/In reaction for transient liquid-phase bonding and 3D chip stacking," *J. Electron. Mater.*, vol. 37, no. 8, pp. 1095–1101, 2008, doi: 10.1007/s11664-008-0487-3.

[2] B. H. L. Chao, X. Zhang, S. H. Chae, and P. S. Ho, "Recent advances on kinetic analysis of electromigration enhanced intermetallic growth and damage formation in Pb-free solder joints," *Microelectron. Reliab.*, vol. 49, no. 3, pp. 253–263, 2009, doi: 10.1016/j.microrel.2009.01.006.

[3] L. Zhang *et al.*, "Materials, processing and reliability of low temperature bonding in 3D chip stacking," *J. Alloys Compd.*, vol. 750, pp. 980–995, 2018, doi: 10.1016/j.jallcom.2018.04.040.

[4] R. M. German, *Liquid Phase Sintering*. Boston, MA: Springer US, 1985.

[5] R.M, *Thermodynamics of Sintering*. Woodhead Publishing Limited, 2010.

[6] J. E. Blendell, W. Lafayette, and U. States, *Solid-State Sintering Solid-State Sintering*, no. April. Elsevier Ltd., 2020.

[7] JOHNSON DL, "Solid-State Sintering," pp. 173–183, 1968, doi: 10.1016/b978-0-08-034720-2.50124-6.

[8] Suk-Joong L.Kang, "Sintering Processes," *Densif. Grain Growth, Microstruct.*, pp. 3–8, 2005, doi: 10.1016/B978-075066385-4/50001-7.

[9] R. M. German, "Thermodynamics of sintering," *Sinter. Adv. Mater.*, pp. 3–32, 2010, doi: 10.1533/9781845699949.1.3.

[10] Y. Zhou, W. F. Gale, and T. H. North, "Modelling of transient liquid phase bonding," *Int. Mater. Rev.*, vol. 40, no. 5, pp. 181–196, 1995, doi: 10.1179/imr.1995.40.5.181.

[11] G. O. Cook and C. D. Sorensen, "Overview of transient liquid phase and partial transient liquid phase bonding," *J. Mater. Sci.*, vol. 46, no. 16, pp. 5305–5323, 2011, doi: 10.1007/s10853-011-5561-1.

[12] D. C. Murray and S. F. Corbin, "Determining the kinetics of transient liquid phase bonding (TLPB) of inconel 625/BNi-2 couples using differential scanning calorimetry," *J. Mater. Process. Technol.*, vol. 248, no. December 2016, pp. 92–102, 2017, doi: 10.1016/j.jmatprotec.2017.05.013.

[13] S. F. Corbin and D. J. McIsaac, "Differential scanning calorimetry of the stages of transient liquid phase sintering," *Mater. Sci. Eng. A*, vol. 346, no. 1–2, pp. 132–140, 2003, doi: 10.1016/S0921-5093(02)00530-0.

[14] M. L. Kuntz, S. F. Corbin, and Y. Zhou, "Quantifying metallurgical interactions in solid/liquid diffusion couples using differential scanning calorimetry," *Acta Mater.*, vol. 53, no. 10, pp. 3071–3082, 2005, doi: 10.1016/j.actamat.2005.03.018.

[15] P. O. Quintero, "DEVELOPMENT OF A SHIFTING MELTING POINT Ag-In PASTE VIA TRANSIENT LIQUID PHASE SINTERING FOR HIGH TEMPERATURE ENVIRONMENTS," University of Maryland, College Park, 2009.

[16] I. Tuah-Poku, M. Dollar, and T. B. Massalski, "A study of the transient liquid phase bonding process applied to a Ag/Cu/Ag sandwich joint," *Metall. Trans. A*, vol. 19, no. 3, pp. 675–686, 1988, doi: 10.1007/BF02649282.

[17] L. Reed-Hill, Robert E.; Abbaschian, Reza;Abbaschian, *Physical Metallurgy Principles*, Fourth. Cengage Learning, 2009.

[18] "Periodic Table." https://periodictable.com.

[19] "MatWeb." http://www.matweb.com/index.aspx.

[20] I. Isomaki, "Tin- Indium Phase Diagram." ASM Alloy Phase Diagram Database, ASM International 2009. Diagram No.102112, 2006.

[21] H. Okamoto, "Tin - Indium Phase Diagram." ASM Alloy Phase Diagram Database, ASM International 2006. Diagram No.901411, 1990.

[22] H. Okamoto, "In−Sn (Indium-Tin)," *J. Phase Equilibria Diffus.*, vol. 27, no. 3, pp. 313–313, 2006, doi: 10.1361/154770306x110032.

[23] T. T. C. Gale, W. F., *Smithells Metals Reference Book*, Eigth Edit. Butterworth-Heinmann, 2004.

[24] J. W. Morris, J. L. F. Goldstein, and Z. Mei, "Microstructure and Mechanical Properties of Sn-In and Sn-Bi Solders," pp. 25–27, 1993.

[25] D. G. Callister, William D, Rethwisch, "Materials Science and Engineering An Introduction," 9th ed., Wiley, 2014, pp. 320–344.

[26] P. F. Hlava, "Indium solder problems," *Microsc. Microanal.*, vol. 12, no. SUPPL. 2, pp. 1072–1073, 2006, doi: 10.1017/S1431927606066049.

[27] R. Kubiak, M. Wołcyrz, and W. Zacharko, "Crystallization, decomposition and superconductivity of β-In3Sn," *J. Less-Common Met.*, vol. 65, no. 2, pp. 263–269, 1979, doi: 10.1016/0022-5088(79)90116-4.

[28] J. L. F. Goldstein and J. W. Morris, "Microstructural development of eutectic Bi-Sn and eutectic In-Sn during high temperature deformation," *J. Electron. Mater.*, vol. 23, no. 5, pp. 477–486, 1994, doi: 10.1007/BF02671233.

[29] Y. Shu, K. Rajathurai, F. Gao, Q. Cui, and Z. Gu, “Synthesis and thermal properties of low melting temperature tin/indium (Sn/In) lead-free nanosolders and their melting behavior in a vapor flux,” *J. Alloys Compd.*, vol. 626, pp. 391–400, 2015, doi: 10.1016/j.jallcom.2014.11.173.

[30] J. W. Morris and M. Engineering, “Microstructure and Creep of Eutectic Indium / Tin on Copper and Nickel Substrates,” vol. 21, pp. 647–652, 1992.

[31] A. Umantsev, “Modeling of intermediate phase growth,” *J. Appl. Phys.*, vol. 101, no. 2, 2007, doi: 10.1063/1.2424530.